Modelling Seasonal and Inter-annual Variations in Carbon and Water Fluxes in an Arid-zone *Acacia* Savanna Woodland, 1981-2012

Running head: **Modelling Variations in Carbon and Water Fluxes**

Chao Chen[1,2,3*], James Cleverly[1,4], Lu Zhang[5], Qiang Yu[1], Derek Eamus[1,4,6]

[1]School of the Environment, University of Technology Sydney, NSW 2007 Australia

[2]National Centre for Groundwater Research and Training (NCGRT), School of Environment, Flinders University, Adelaide, SA, 5001, Australia

[3]CSIRO Agriculture Flagship, PMB 5, PO Wembley, WA 6913, Australia

[4]Australian Supersite Network, Terrestrial Ecosystem Research Network, University of Technology Sydney

[5]CSIRO Land and Water, CSIRO Water for a Healthy Country National Research Flagship, GPO Box 1666, Canberra, ACT, 2601, Australia

[6]National Centre for Groundwater Research and Training, University of Technology Sydney, NSW 2007, Australia

[*] Phone: +61 8 9333 6672; Email: chao.chen@csiro.au

ABSTRACT

Changes in climatic characteristics such as seasonal and inter-annual variability may affect ecosystem structure and function, hence alter carbon and water budgets of ecosystems. Studies of modelling combined with field experiments can provide essential information to investigate interactions between carbon and water cycles and climate. Here we present a first attempt to investigate the long-term climate controls on seasonal patterns and inter-annual variations in water and carbon exchanges in an arid-zone savanna-woodland ecosystem using a detailed mechanistic soil-plant-atmosphere model (SPA), driven by leaf area index (LAI) simulated by an ecohydrological model (WAVES) and observed climate data during 1981−2012. The SPA was tested against almost three years of eddy covariance flux measurements in terms of gross primary productivity (GPP) and evapotranspiration (ET). The model was able to explain 80% and 71% of the variability of observed daily GPP and ET, respectively. Long-term simulations showed that carbon accumulation rates and ET ranged from 20.6 g C m^{-2} mon^{-1} in the late dry season to 45.8 g C m^{-2} mon^{-1} in the late wet season, respectively, primarily driven by seasonal variations in LAI and soil moisture. Large climate variations resulted in large seasonal variation in ecosystem water-use efficiency (eWUE). Simulated annual GPP varied between 146.4 and 604.7 g C m^{-2} yr^{-1}. Variations in annual ET coincided with that of GPP, ranging from 110.2 to 625.8 mm yr^{-1}. Annual variations in GPP and ET were driven by the annual variations in precipitation and vapour pressure deficit (VPD) but not temperature. The linear coupling of simulated annual GPP and ET resulted in eWUE having relatively small year-to-year variation.

Keywords: Gross primary production; Evapotranspiration; Transpiration; Water-use efficiency; WAVES model; SPA model.

INTRODUCTION

Climate and its variability play an important role in mediating the structure and function of terrestrial ecosystems because of the close association between the carbon and hydrological cycles (Baldocchi 1997; Williams and others 2001a). It has been predicted that climate will change at both regional and globe scales and thus patterns of precipitation, temperature, solar radiation and vapour pressure deficit (VPD) may vary seasonally (Houghton and others 1996; IPCC 2014). Year-to-year variability under a future warmer climate is also expected to be larger (Salinger 2005). These changes in climate are likely to affect terrestrial ecosystem uptake of atmospheric CO_2 and the hydrological cycle. Understanding the responses of hydrological and plant physiological processes in terrestrial ecosystem to climate variations is of importance to rangeland and water resource managers, particularly in arid and semi-arid regions, such as arid-zone savanna woodlands.

Savannas are among the most striking vegetation types, located in tropical and sub-tropical zones that contain a discontinuous tree canopy with a substantial grass understory (Eamus and Prior 2001). These ecosystems occupy a large proportion of global land area (about 20%) and significantly contribute to regional and continental-scale carbon and water budgets. Savannas experience large variations in temperature, moisture availability and sunlight, which are controlling factors of the ecosystem CO_2 exchange (Baldocchi 2008; Wohlfahrt and others 2008; Yan and others 2011; Cleverly and others 2013) and water fluxes (Eamus and others 2013b). This is particularly the case in Australia, the driest permanently inhabited continent on Earth (Eamus 2003), where savannas cover approximately 25% of the continent.

Due to the remoteness of Australia's interior, however, studies that investigate the controls exerted

by climate on water and carbon dynamics have only recently been undertaken in Australian arid-zone savannas (Cleverly and others 2013; Eamus and others 2013b). The climate of the region is characterized by a distinct wet season (Nov–Feb) accounting for 75–80% of annual precipitation (Eamus and others 2013b), but with a long period (up to four months) of no rainfall in the dry season. These field experiments were conducted over a period of about 2 years and provided useful information on carbon and water dynamics in the arid-zone savannas. However, long-term studies of carbon and water fluxes are needed to understand seasonal and inter-annual relationships between climate and the exchanges of carbon and water.

Detailed process-based simulation models are valuable tools to integrate knowledge of climate, plant processes and hydrology and scale these processes to stand and ecosystem levels (Williams and others 1996; Landsberg and Coops 1999; Braswell and others 2005). The soil-plant-atmosphere (SPA) model is a process-based model that is able to simulate ecosystem photosynthesis, energy balance and water transport. The model was designed for direct comparisons with eddy covariance (EC) estimates of carbon and water fluxes and has been successfully implemented in temperate (Williams and others 1996, 2001a), tropical (Williams and others 1998) and arctic (Williams and others 2000) ecosystems, including recent applications in Australian ecosystems (Zeppel and others 2008; Whitley and others 2011; Eamus and others 2013a). In one example from a temperate ecosystem, Schwarz and others (2004) concluded that SPA was suitable for simulating seasonal and annual responses of gross primary productivity (GPP) and transpiration (T) to climate variability in seasonally drought-affected Ponderosa pine forests. Likewise in the present study we applied the SPA model to investigate climatic controls on GPP and evapotranspiration (ET) in a Mulga-dominated landscape.

The SPA model requires daily leaf area index (LAI) as an input. In contrast to the soil, plant physiological and meteorological parameters, it is difficult to obtain daily LAI for long-term simulations (e.g. 30 years). The water-atmosphere-vegetation-energy-soil (WAVES) is a model based on the biophysical processes within the soil-vegetation-atmosphere system (Zhang and others 1996; Zhang and Dawes 1998). In the model, carbon assimilation, allocation and respiration are dynamically estimated from empirical relationships with the availability of light, water, nutrients and ambient CO_2 concentration, which allows LAI to vary with environmental conditions. Hence, daily LAI was simulated by the WAVES model and was used as an input to the SPA model in this study.

The ecosystem water-use efficiency (eWUE) can be expressed as net ecosystem exchange (NEE) or GPP to ET (Beer and others 2009; Perez-Ruiz and others 2010; Linderson and others 2012). It is an important index representing the trade-off between carbon uptake and water loss and provides a metric for evaluating ecosystem productivity and resilience (Baldocchi 1994; Ponce-Campos and others 2013). Alternative to eWUE, inherent WUE (IWUE), calculated as the ratio of GPP × VPD to ET (Eamus and others 2013b) can be used to examine the intrinsic link between carbon and water fluxes through stomatal conductance at the ecosystem level. Studies of eWUE and IWUE have indicated that they respond differently between wet and dry years (Ponce-Campos and others 2013) and wet and dry seasons (Eamus and others 2013b). Thus the work described herein also examined the responses of eWUE and IWUE to historical climate variations at both seasonal and inter-annual scales in this savanna woodland ecosystem.

The objectives of this study were to: (1) parameterize and validate the SPA model using almost three years of eddy covariance measurements and LAI simulated by WAVES in a landscape of

central Australia dominated by a N-fixing tree, Mulga (*Acacia aneura*); and (2) quantify and explain seasonal and interannual variability of carbon- and water fluxes under historical climate variations, in terms of GPP, ET and WUE. The primary purpose of this study was to test the hypotheses that seasonal variations of GPP, ET and WUE of this mulga-dominated landscape are controlled principally by temperature and VPD, not precipitation considering the fact that precipitation has relatively less seasonal variation with the dominant pattern of summer rainfall (Nov–Feb; Eamus and others 2013b); while the large variations in inter-annual precipitation (Chen and others 2014) affect GPP, ET and eWUE at an inter-annual time scale. As far as it is known to the authors, this is the first attempt to explore seasonal and inter-annual dynamics of carbon and water fluxes for this ecosystem over a long time period (1981–2012). Such information is critical to estimating future changes to carbon sink-source status and hydrological cycles associated with changes in climate in arid-zone Australia.

MATERIALS AND METHODS

Study Site

The site selected for this study is in central Australia, located approximately 200 km north of Alice Springs, NT (22.283S, 133.249E and a.s.l. 600 m). Climate in this region is characterized by hot summers and warm winters in the arid tropics. In the past 32 years (1981–2012), summer maximal temperature (46.2 ^{o}C) occurred in Jan and winter minimal temperature (-4 ^{o}C) was reached in Aug in 1994 at the nearest meteorological station (Territory Grape Farm; Eamus and others 2013b). Large variation in inter-annual precipitation occurs here, ranging from 97.4 to 832.9 mm yr^{-1}, with an average of 326.0 mm yr^{-1}. Precipitation is also highly seasonal, with about 75–80% of rainfall occuring during the wet season (Nov–Apr; Bowman and others 2010). The soil is characterised as

a red kandosol. The ecosystem is an Mulga (*Acacia neura*) savanna woodland with an average canopy height of 6.5 m above an understory dominated by C4 warm-season grasses that is dependent upon rainfall (Cleverly and others 2013).

Experimental Data for Testing the SPA and WAVES Models

An eddy covariance tower, a member of the OzFlux network (http://www.ozflux.org.au/; Cleverly 2011), was located on a flat plain between the Hanson and Woodforde Rivers. Potential fetch is 11 km to the east and 16 km to the south. EC data were initiated on 2 September 2010 and collected from a 13.7 m tower. The three-dimensional eddy covariance system was mounted 11.6 m above the ground, facing into the predominant south-east wind direction (Chen and others 1991), and consisting of a CSAT3 three-dimensionalsonic anemometer (Campbell Scientific Australia, Townsville, QLD, Australia) and a LiCor 7500 open-path infrared gas analyser (JohnMorris, Chatswood, NSW, Australia). Air temperature and relative humidity were measured using an HMP45C (Vaisala, Helsinki, Finland) at the height of 11.6 m above the ground. Four-component net radiation was measured at 12.2 m above the ground with a CNR1 (Kipp & Zonen, Delft, The Netherlands). Precipitation was measured with a CS7000 (Hydrologic services, Warwick, NSW, Australia), centred in a 10 m × 15 m clearing (about 15 m from the eddy covariance tower) at the top of a 2.5 m mast. Flux measurements were made at frequency of 10 Hz with a 30-minute covariance interval.

An AMS Soil Core Sampler (The Environmental Collective, Auckland, New Zealand) was used to extract intact cores (38 mm diameter × 10 cm depth to a maximum depth of 1.4 m) for laboratory analysis. A fairly uniform soil profile was indentified with bulk density varying only slightly from 1.67 g cm^{-3} at the surface to 1.86 g cm^{-3} at a depth of 1.4 m. A soil column of 4 m was chosen to

simulate the relatively shallow rooting depth for Mulga at this site.

To calibrate the WAVES model, LAI was derived from images acquired with a digital camera (Canon DSLR). Five 100 m long transects were established in the tower footprint (NE to SW). To compute LAI for the canopy (Mulga), images were acquired with the camera oriented toward zenith (to the sky, 0^{o}). These canopy images were analyzed in Matlab (R2012, The Mathworks, Natick, MA, USA) using the method of MacFarlane and others (2007). To compute understory LAI, photographs were oriented toward the soil at an angle of 57.5^{o} from nadir (Weiss and others 2004) and analyzed with CANEYE (V6.3, https://www4.paca.inra.fr/can-eye), based on the method proposed by MacFarlane and others (2007). Total LAI was calculated as the sum of the canopy and understory components.

A more detailed description of field measurements and data processing can be found in Cleverly and others (2013) and Eamus and others (2013b).

Forcing Energy Balance Closure

The use of flux data to validate biophysically-based models requires that conservation of energy is satisfied as it is defined in the model (Twine and others 2000; Chen and others 2014). To force energy balance closure, energy is generally added into the turbulent term [H+λE] (where H and λE are sensible and latent heat fluxes, respectively) of the closure ratio D ([H+λE]/[R_n-G-S], where R_n is net radiation, G is ground heat flux and S is heat storage) in proportion to the measured Bowen ratio (H/λE). In practice, energy in semi-arid regions is returned to H when ET is small and into λE during the days following rainfall when λE is large and H is limited by cloud cover. In the present study, S was relatively minor and neligible due to the minimal biomass density of short canopies (Wilson and others 2002). Therefore, the energy balance was closed each half-hourly period by

attributing the residual energy to H and λE according to the observed Bowen ratio in that half hourly period.

SPA Model

The SPA model is a process model (Williams and others 1996) that was designed for direct comparisons with eddy covariance estimates of carbon and water fluxes (GPP, ET and T) and can simulate ecosystem photosynthesis, energy balance and water transport at fine temporal and spatial scales (Williams and others 2001b). The original model has 20 soil layers to simulate root distribution and soil-water uptake and has 10 canopy layers to simulate C3 vascular plant processes at a 30-min time step. The ecosystem structure is described by vertical variations among canopy layers in light absorbing leaf area, photosynthetic capacity, and plant hydraulic properties (Williams and others 2001a). Because of the significant contribution of C4 grasses to total LAI during the wet season in tropical savannas, Whitely and others (2011) added a C4 photosynthesis module to simulate understory grasses. The modified SPA model was used here. Photosynthesis process for C3 trees is predicted by using the C3-photosynthesis model of Farquhar and others (1980), and the simplified C4 photosynthesis model as described by Collatz and others (1992) is used to determine the C4 net assimilation rate. The model contains 10 canopy layers. The model user can define the layers accounted for by C_3 trees and C_4 grass based on the contribution of the tree or grass to total LAI. ET and T are determined by the Penman-Monteith equation (Monteith and Unsworth 2008), in which surface conductance is derived internally from the optimal stomatal conductance that is adjusted to maximize daily carbon uptake per unit of foliar nitrogen and maintain vapour exchange beneath a threshold maximum to avoid cavitation of the hydraulic system (Williams and others 1996). Water loss is determined by the water potential gradient

between leaf and soil, liquid phase hydraulic resistances and the capacitance of the pathway from soil to leaf. Detailed information on the parameterization of the model is given in Table 1. More detailed descriptions of the fundamental equations, model logic, algorithms and the development history of the SPA model were given by Williams and others (1996, 1998, 2001a) and Whitely and others (2011).

SPA is one of the most widely and successfully applied land surface exchange models and has been tested across a range of diverse ecosystems such as Arctic tundra (Williams and others 2001a) and Brazilian tropical rainforests (Fisher and others 2007). The model driven by observed LAI has also been tested and used for simulating carbon and water cycle components in woodland of arid and semi-arid Australia (Zeppel and others 2008; Whitley and others 2011). These applications of the SPA model indicate that model simulation can explain at least 60% of the variation in carbon and water fluxes in these tested areas. However, it is difficult to obtain daily LAI values at long-time scale, which limits the application of the model for the long-term simulations.

WAVES Model

WAVES is an ecohydrological model (Dawes and Hatton 1993; Zhang and others 1996) that adopts a one or two layer canopy representation with a soil layer underneath. In WAVES, the micrometeorological interactions between canopy and atmosphere are regulated by the omega coefficient proposed by Jarvis and McNaughton (1986). The model includes estimates of carbon storage and allocation between leaves, roots and stems as in Running and Coughlan (1988). The daily carbon assimilation rate is estimated by the maximum carbon assimilation rate and relative growth rate multiplicatively, the former of which is a species dependent parameter reported for C3 palnts by Collatz and others (1991) and C4 by Collatz and others (1992). Assimilation is allocated

according to the priorities of maintenance respiration, growth respiration, leaf and root growth, and stem growth. Leaf area increase is determined by carbon allocated to leaves and specific leaf area, and root growth is determined by the allocated carbon that is distributed amongst soil nodes weighted by the availability of soil water and nutrients following the methodology of Wu (1994). The physiological responses of canopy conductance and assimilation rate are fully coupled with climatic regulation on stomata and water and nutrients availability to roots, which allows LAI to vary with different environmental conditions. The WAVES model has been proven to be able to successfully reproduce vegetation structure (e.g. LAI) from field observations (Zhang and others 1999; Wang and others 2001; Shao and others 2002). However, WAVES is an ecohydrological model, not a process-based carbon model. It does not explicitly simulate full carbon cycle and nor does it provide direct GPP estimates, the latter of which is one of the objectives of this study. As with SPA, ET was estimated by the Penman-Monteith approach (Monteith and Unsworth 2008) in WAVES. A more detailed description of WAVES is provided in Zhang and others (1996), Dawes and others (1998) and Zhang and Dawes (1998).

We recently successfully parameterized and tested WAVES for this site (Chen and others 2014), using the same flux data as used in the present study. Although MODIS reflectance data are often noisy, LAI modeled with WAVES agreed reasonably well with measured and MODIS LAI, derived from the MOD15A2 product (8-Day Composite, 1 km wide × 1 km high) centered on the coordinate of the tower (http://daac.ornl.gov/MODIS/). The model was able to explain about 93% of the variation in observed understory LAI (0.04 RMSE) and 65% of the variation in the canopy LAI (0.05 RMSE, Fig. 1). In the simulation, the coefficient of determination of simulated and measured canopy LAI was smaller than that for the understory (Chen and others 2014), due to

extreme variability in leaf physiology, water status and responses to moisture and heat stress of Mulga as a "stress endurer" (Winkworth 1973; O'Grady and others 2009; Cleverly and others 2013; Eamus and others 2013b). This was also because LAI was optimized to maintain a better match between simulated and measured values of ET. Generally speaking, the calibrated WAVES model can be used confidently to simulate vegetation growth in the study area. Thus in the present study, we firstly used the parameterized WAVES model to obtain the dynamics of LAI for the period of 1981-2012, and then by using the LAI output from WAVES as an input for SPA, the SPA model was used to quantify the response of water and carbon fluxes to climate variability at this Mulga site during 1981–2012. The combination of the two models enabled us to estimate carbon and water fluxes under different climatic and vegetation characteristics by taking the advantages of each model.

The SPA Model Evaluation

The EC flux data during 3 Sep 2010−30 Jun 2013 were used to evaluate the performance of the SPA model in simulating water and carbon fluxes under variable climate conditions in terms of ET and GPP. We divided these data into two datasets. The data obtained between 3 Sep 2010 and 31 Dec 2011 were used to parameterize the model; those obtained during 1 Jan 2012 and 30 Jun 2013 were used to validate the model. Model inputs and their values and source of this study were shown in Table 1. Three indices were used to evaluate the performance of the SPA model: i) the coefficient of determination (r^2), describing the proportion of the variance in measured data explained by the model; ii) the root mean square error (RMSE), providing a measure of the absolute magnitude of the error; and iii) model efficiency (ME), presenting variation in measured values accounted for the model. The indices were calculated as follows:

$$\text{RMSE} = \sqrt{\frac{1}{n}\sum_{i=1}^{n}(P_i - O_i)^2} \quad (1)$$

$$ME = 1 - \frac{\sum_{i=1}^{n}(P_i - O_i)^2}{\sum_{i=1}^{n}(O_i - O_{avg})^2} \quad (2)$$

Application of the SPA Model for Long-term Simulations

The validated SPA model was then applied to simulate the responses of carbon and water fluxes in the arid-zone *Acacia* savanna woodland to historical climate variability (1981–2012). For application of the SPA model, meteorological data at half-hourly intervals are needed. To meet this requirement for long-term simulation, daily climate data during 1981–2012 at Territory Grape Farm, extracted from SILO (Jeffrey and others 2001; http://www.bom.gov.au) were interpolated into half-hourly intervals. To do this, firstly, the half-hourly meteorological data (temperature, solar radiation, rainfall or VPD) during Sep 2010–Jun 2013 measured at an on-site meteorological station were obtained. Secondly, these measured half-hourly meteorological data were examined and fitted to determine the daily climatological cycle of each climate variable at an half-hourly time step, using a fourth-order polynomial regression. Thirdly, the measured half-hourly meteorological data were converted into daily values for each day of the entire period (Sep 2010–Jun 2013) and then these values were averaged to obtain a daily climatology for each climate variable. Finally, the fitted curve of each climate variable obtained in the second step was used to re-scale the 32 years of meteorological data to obtain long-term half-hourly meteorological data, by multiplying the ratio of the daily value during 1981–2012 to the daily average obtained in the third step. Due to the lack of local CO_2 concentration values, global monthly CO_2 concentration values during 1981–2012 were used for each 30 minutes during the corresponding

month of the year. Moreover, the average annual cycle of half-hourly wind speed during the field experimental period was used for all the 32 years due to unavailability of wind speed data at this remote meteorological station.

RESULTS

Model Performance

The comparisons of simulated ET and GPP with the corresponding measurements obtained from the field experiment during 3 Sep 2010−30 Jun 2013 are shown in Fig. 2. In general, the model was able to capture periods of very low and peak values of measured daily ET, which ranged from 0.0 to 5.93 mm with an average of 1.15 mm, compared to the simulated ET that ranged from 0.0 to 5.31 mm with an average of 1.29 mm (Fig. 2a). The SPA model was also able to capture periods of low and peak daily GPP and replicate seasonal and annual patterns of derived GPP closely (Fig. 2b). Values of GPP derived from EC measurements ranged from 0 to 5.57 g C m^{-2} d^{-1} with an average of 1.52 g C m^{-2} d^{-1}, with maximum values occurring in March and minima in July. Maximal and minimal GPP simulated by SPA also occurred in March and July, respectively. The modelled GPP ranged from 0.09 to 5.43 g C m^{-2} d^{-1} with an average of 1.49 g C m^{-2} d^{-1}.

The model simulated carbon and water fluxes with acceptable accuracy and precision. There was a significant positive relationship between simulated and observed ET across the field observational period (Table 2), with r^2 of 0.71 and RMSE of 0.86 mm d^{-1}, although the model slightly overestimated ET by 12.2% due to an overestimation of LAI values (Fig. 1). This overestimation resulted from maintaining a match between modelled and measured values of ET in WAVES that has the difficulty in capturing the extreme variability in leaf physiology, water status and responses to moisture and heat stress of Mulga as a “stress endurer” (Chen and others 2014). The model

explained 80% of the variation in daily GPP, with a RMSE value of 0.45 g C m^{-2} d^{-1}. The values of ME were close to 1 for both GPP and ET.

Seasonal Patterns in Carbon and Water Fluxes

The climate at this site is characterized by two distinct seasons: hot-wet summer (Dec–Feb) and warm winter (Jun–Aug; Fig. 3). During the observation period monthly mean temperatures ranged from 13.6 ^{o}C in July to 29.8 ^{o}C in January (Fig. 3a), while monthly mean solar radiation varied between 15.9 in June and 26.2 MJ m^{-2} d^{-1} in January (Fig. 3b). About 55% of precipitation fell in the three summer months (Dec to Feb, Fig. 3c). VPD in the summer was almost three times larger than in the winter (Jun to Aug; Fig. 3d) as a result of high temperatures that compensated for the large absolute humidity during the summer. The largest total monthly GPP (48.5 g C m^{-2}) occurred in March (Fig. 4a), reflecting the influence of high (relative to winter values) soil water content arising from summer rainfall coupled with moderate temperature and solar radiation in this month (relative to higher values in January and much lower values in June; Fig. 3). From March through to September, ecosystem GPP declined exponentially to a minimum of 20.6 g C m^{-2} mon^{-1}. Simulated ET also displayed strong seasonal variations (Fig. 4b). The largest total monthly ET occurred in February (46.2 mm) due to the effects of summer rainfall, high temperature and high VPD in this month. After reaching maximum values in February, ET showed an approximately exponential decline to a minimum monthly value of 11.5 mm in September.

Using the SPA model with LAI outputs from the WAVES model as inputs, landscape carbon and water fluxes for the C3 overstory and C4 understory were disaggregated. During the wet season (Nov to Mar), simulated total monthly GPP ranged between 23.4 and 48.5 g C m^{-2}, of which the C3 tree overstory accounted for 62–86% and C4 grass understory contributed 14–38% (Fig. 4c).

Over the same period, the water transpired by the C3 overstory accounted for about 66–81% of the total water-use (ET), while C4 understory accounted for approximately 8–23% (Fig. 4d). During the dry season (Jun to Sep), almost all carbon and water fluxes were accounted for by the C3 component of the vegetation (Fig. 4c, d), as there was little C4 leaf area or biomass to support any carbon and water fluxes.

Inter-annual Variability in Water and Carbon Fluxes

Climatic conditions in the last 32 years were highly variable with large fluctuations in precipitation (97.4–832.5 mm yr^{-1}; Fig. 5c). Annual mean VPD showed moderate variation, ranging from 1.3 to 2.1 kPa (Fig. 5d). Likewise, variations in annual mean temperature (21.2–23.4 ^{o}C) and solar radiation (20.7–23.1 MJ m^{-2} d^{-1}) were relatively small (Fig. 5a, b). Such inter-annual climate variability resulted in GPP ranging between 146.4 and 604.7 g C m^{-2} yr^{-1} (standard deviation of 97.6 g C m^{-2} yr^{-1}) over the 32-year period (Fig. 6a). C3 trees were estimated to contribute more than 75% of total GPP in 85% of 32 simulated years. In contrast, average annual GPP of C4 grass understory accounted for 20% of total GPP due to its short growing season and small LAI. The annual total ET from the *Acacia* savanna woodland was simulated to vary between 110.2 and 625.8 mm yr^{-1} over 32 years, with a standard deviation of 114.2 mm yr^{-1} (Fig. 6b). Annual patterns of simulated GPP (Fig. 6a) closely matched those in simulated annual ET (Fig. 6b). Simulated T of the C3 overstory ranged from 74.3 to 459.2 mm yr^{-1}, accounting for 60–73% of the estimated ET. In contrast, the simulated water transpired by C4 grasses only accounted for 6–17%.

Ecosystem Water-Use-Efficiency and Inherent WUE

We used SPA outputs to estimate water-use-efficiency at the ecosystem scale (eWUE, calculated as GPP/ET; Perez-Ruiz and others 2010) and inherent WUE (IWUE; calculated as GPP*VPD/ET;

Eamus and others 2013b) (Figs. 7, 8), eWUE for C3 trees (C3 WUE, calculated as GPP/T) and C4 grasses (C4 WUE, calculated as GPP/T) (Figs. 7, 8). Monthly mean eWUE showed strong seasonal variations, with values ranging from 0.77 to 1.88 g C m^{-2} (mm water)$^{-1}$ with a standard deviation of 0.42 g C m^{-2} (mm water)$^{-1}$ (Fig. 7). Even larger variation was found for IWUE, varying between 1.26 to 3.39 g C m^{-2} (mm water)$^{-1}$ with a standard deviation of 0.61 g C m^{-2} (mm water)$^{-1}$. The average values of eWUE and IWUE were 1.28 to 2.17 g C m^{-2} (mm water)$^{-1}$, respectively. The mean monthly WUE of C4 grasses was always larger than that of C3 trees (37% on average).

Annual mean eWUE varied between 0.75 and 1.59 g C m^{-2} (mm water)$^{-1}$ during 1981-2012, with an average of 1.17 g C m^{-2} (mm water)$^{-1}$ (Fig. 8). The lower eWUE usually occurred in wet years when VPD was small, and *vice versa*. Thus, due to the effects of inter-annual variability in VPD, compared with that of eWUE, inter-annual variations of IWUE were enlarged, in which the range increased from 1.1 to 3.3 g C m^{-2} (mm water)$^{-1}$. The average value of eWUE (1.1 g C m^{-2} (mm water)$^{-1}$) was smaller than that for IWUE (2.2 g C m^{-2} (mm water)$^{-1}$.

The inter-annual variation of eWUE for C3 trees was similar to that of eWUE due to the large proportion of annual GPP and T by C3 vegetation (Fig. 8). Compared with eWUE and C3 WUE, C4 WUE showed largest inter-annual variability with a range of 1.11 to 3.06 g C m^{-2} (mm water)$^{-1}$.

DISCUSSION

The Simulation Models and Data Extrapolation

Understanding carbon–water relations in arid-zone woodland ecosystems is important for improving land and water management within the limitations of the ecohydrologic system. A modeling approach is especially effective in examining the patterns and drivers in complex fluxes

across long timescales because conducting field experiments and maintaining a field-based flux measurement system in remote regions is difficult and expensive. This study presents a first attempt to explore the long-term temporal dynamics of water and carbon cycles in an arid-zone savanna-woodland ecosystem by combining an ecohydrological model, WAVES, that simulates the dynamics of vegetation growth and development, with a detailed mechanistic soil-plant-atmosphere model, SPA. Land surface exchange models that simulate long-term fluxes usually require such input variables as LAI (Baldocchi and Wilson 2001), which is difficult to obtain at fine- and long-time scales. Thus, attempts to model carbon dioxide and water vapour exchange over decadal time-scales often require linked ecophysiological models that provide information on parameters related to vegetation growth (especially LAI).

The first objective of this study was to parameterize and test SPA against eddy covariance data. The large ME and small RMSE values for simulated ET and GPP show that the SPA model, driven by LAI values provided by the WAVES model, is able to reproduce the responses of water and carbon fluxes of the woodland ecosystem to climate variability. Although experimental data used to test the model was only over a 3-year period, this time period contained two years of contrasting rainfall. The first year was wet (>250 mm above average rainfall), while little precipitation (>100 mm below average) fell during the second year (Cleverly and others, 2013). As such, we have reason to believe that the parameters calibrated for the experimental period are suitable to others years. This combination of two process-based models has the potential to provide answers to questions concerning the role of climate on ecosystem water and carbon balances. To use the calibrated model to analyse carbon and water fluxes of the last 32 years, we first interpolated daily climate data for 32 years into half-hour

intervals to meet the requirement of the SPA model. Some interpolation errors may result from the assumption that each climate variable (temperature, solar radiation, precipitation or vapour presser deficit) had the same daily cycle throughout the study period. In addition, because of a lack of long-term wind speed data, we assumed the 32-year wind speed was the same as the observed half-hour wind speed climatological cycle. Such assumptions are possibly a major source for uncertainy in simulated GPP and ET at half-hour resolution. A sensitivity analysis showed that a 50% of decrease in wind spead would result into about 2% decrease in simulated ET and 2% increase in simulated GPP, while a 50% of increase in wind spead would decrease about 14% of ET and decrease about 17% of GPP. These uncertainties may further affect eWUE (-4% − 5%) at this time scale. However, being restricted by data availablility this study aims to make a first attempt to explore seasonal and inter-annual dynamics of carbon and water fluxes for an arid-zone savanna ecosystem in the remoteness of Australia's interior over such a long time period (1981–2012). We argue that our results of simulated GPP and ET at seasonal and inter-annual scales are reliable, despite those uncertainties, as the daily average of interpolated climate variable were still kept the same as the original daily average.

Seasonal Fluxes of GPP and ET and the Relative Contributions of C3 Trees and C4 Grasses (1981-2012)

Simulated GPP and ET were smallest at the end of the dry season (Sep) and highest in the wet season (Feb–Mar; Fig. 4). Although showing a similar seasonal cycle, a linear regression fit of temperature, solar radiation and VPD with GPP and ET indicates a low correlation with the coefficient of determination (r^2) varying between 0.001 to 0.23 for GPP and 0.19 to 0.70 for ET (Table 3). In contrast, the correlations between GPP and ET with the LAI and the soil water content

were much stronger at a seasonal timescale (r^2 values $\geq$ 0.72; Fig. 9). Thus, meteorological variables are only indirectly related to GPP and ET at the seasonal time-scale. Consequently, our first hypothesis that temperature and VPD would explain the seasonal variability of GPP and ET was rejected. We conclude that it is not the direct influence of climate variables on leaf physiology *per se* that causes seasonal changes in GPP and ET of the savanna ecosystem but variations in LAI and soil water that are important. Whereas, by contrast, Migliavacca and others (2009) showed that, during summer, a significant reduction of net productivity of a poplar plantation under peculiar eco-climatic conditions was mainly driven by high temperature even in absence of marked soil water stress. Tian and others (2000) found that seasonality in precipitation (but not temperature), especially the amount received during the drier months, was an important control on net ecosystem production in the undisturbed ecosystems of the Amazon Basin.

Changes in total LAI were found predominantly in the C4 understory, in which physiological activity is restricted to the summer (Fig. 10). Consequently, despite having a lower contribution to the total green biomass, the understory plays a significant role in shaping the seasonality of the LAI. The months of peak LAI in the understory (Jan–Feb) coincided with peaks in temperature, precipitation and VPD (Chen and others 2014). In contrast, GPP and T peaked in March (Fig. 4) after precipitation had mostly ceased, temperature and VPD were moderate, and canopy LAI was near a minimum (Fig. 10). Mulga GPP and T were relatively small during December through February (Fig. 4) due to extreme high temperature (Nix and Austin, 1973) and VPD (Eamus and others 2013b). However, they were even smaller during July through September due to low precipitation and hence reduced soil moisture content. By the end of the winter dry season, soil moisture content declined to a minimal value, which was associated with a decline in stomatal

conductance and photosynthetic rate of savanna species generally, including Mulga trees (Eamus and Cole 1997; O'Grady and others 2009; Cleverly and others 2013). The combined effects of minimal understory LAI and declining soil moisture content resulted in little ET and GPP towards the end of the dry season, when Mulga growth was also restricted. In brief, seasonal variability of GPP and ET was driven by LAI and soil moisture in this arid-zone Acacia savanna woodland.

Simulated wet season productivity accounted for approximately 50% of total annual productivity as a result of the large contribution by C4 grasses to total LAI and wet soil due to summer precipitation control, which were the main factors to affect GPP (Fig. 9).

Due to the high water stress tolerance of Mulga trees (O'Grady and others 2009), they remain photosynthetically active in the dry season (although dropping a large percentage of their green leaf area), thus, contributing 5.7 times more to the total annual GPP compared to the annual C4 grasses. Approximately 62% of annual ET occurred in wet seasons, of which T of C3 trees accounted for 66% and that of C4 grasses accounted for 11%. Although C4 grasses contributed a relatively small proportion of ecosystem ET across the wet season, those contributions were disproportionately focused on sub-seasonal periods of wet soils, high temperature and large VPD (Nix and Austin 1973).

Inter-annual Variation of GPP and ET and the Relative Contributions of C3 Trees and C4 Grasses (1981-2012)

Climate in the last 32 years varied with large fluctuations in precipitation, radiation, temperature and VPD due to the effects of the Australian monsoon depressions (Kong and Zhao 2010; Berry and others 2011). Years with large amounts of precipitation also experienced reduced temperature, solar radiation receipt and VPD (Fig. 5), illustrating the control exerted by precipitation and cloud

cover on temperature and VPD at an annual timescale (Cleverly and others 2013). Correlation analysis showed that variations in annual GPP and ET were significantly related to inter-annual variations of annual precipitation, and to a lesser extent VPD (Fig. 11). Our results therefore showed that inter-annual variability of annual GPP in savanna woodland ecosystem is functionally more dependent on precipitation and VPD than temperature. In other words, inter-annual variability of GPP and ET is driven by differences in precipitation and VPD, as concluded by Eamus and others (2013b). This is in contrast to other cooler ecosystems such as boreal forests, in which annual GPP is positively correlated with mean annual air temperature (Law and others 2002; Nemani and others 2003). This is because mean annual temperature in the present study is higher than the threshold of 20 ^{o}C (Fig. 5), above which GPP is generally insensitive (Wang and others 2008). As a result of high inter-annual variability in precipitation (Fig. 5c) and VPD (Fig. 5d), simulated annual ET and GPP differed substantially between dry years (years when precipitation was below 25% of the precipitation percentiles from 1981 to 2012) and wet years (years when precipitation was larger than 75% of the precipitation percentiles from 1981 to 2012; Fig. 12).

Simulated annual ET varied between 110.2 to 625.8 mm, which accounted for 74–134% (97% on average) of annual rainfall ranging from 97.4 to 832.5 mm. The over 100% values of the ratio of annual ET to annual rainfall indicate that there was carry-over of water stored in the soil from one year to the next (Fig. 13a, b). Our simulation results showed that this time lagged response happened in 32% of simulated years and could be sustained up to three continuous years (data not shown). Such time lagged responses have previously been demonstrated in semi-arid grasslands and woodlands (Flanagan and others 2011; Raz-Yaseef and others 2012). The use of water that was released from storage in a different year from which it entered was largest when a relatively wet

year was followed by a dry year. Carry-over of soil moisture is possible in this area due to the patchy but extensive hardpan that underlies central Australian red kandosols within rooting depths (Morton and others 2011). The sub-surface hardpan prevents rainfall from generating deep drainage and thereby increases the duration for which water is available to vegetation. As an evergreen "stress endurer" (Winkworth 1973; O'Grady and others 2009; Cleverly and others 2013; Eamus and others 2013b), Mulga can maintain positive rates of photosynthesis and T in drought years by having access to soil moisture that was stored during antecedent wet years.

Studies showed that, in the tropical eucalypt savannas of northern Australia (annual average rainfall of 1750 mm), C3 vegetation accounted for approximately 60% of the total annual GPP and T of C3 trees contributed about 57% of total annual ET, while C4 grasses contributed 40% and 11% to total annual GPP and ET, respectively (Whitley and others 2011). In contrast, in this study C3 trees accounted for 81% and 71% of the total annual GPP and ET in the semi-arid Mulga woodland region during the 32 years of study period (1981–2012), with C4 grasses contributing 19% of total GPP and T of C4 grasses being 11% of annual total ET (Fig. 6). Even though their annual average contributions to GPP and ET are relatively small due to the large variability in rainfall, the contributions by C4 grasses to annual carbon and water budgets should not be ignored because photosynthesis and T in the understory occur during the summer when GPP in the C3 trees is still minimal (Fig. 5).

Ecosystem Water-Use Efficiency and Inherent WUE

Determinations of the temporal pattern of the WUE in arid-wood land ecosystem is an important contribution to our understanding of the carbon-water relations of these systems. Whitley and others (2011) discussed the seasonal and inter-annual patterns of ecosystem WUE in mesic

savannas for 5-year period. By contrast, we explored seasonal and inter-annual dynamics of ecosystem WUE over a longer time period (1981–2012) in a semi-arid woodland savanna. Our results showed that eWUE was much higher (56% increase) in the dry season than the corresponding value in the wet season (Fig. 7). This is because that the relative magnitude difference in GPP between wet season and dry season (Fig. 4a) was much smaller than that in ET between the two seasons (Fig. 4b). This arose because of the maintenance of a modest GPP and a much reduced ET of the Mulga in the dry season. The smaller eWUE values in the wet season resulted from higher VPD, higher temperature and relative more precipitation that increased ET more than GPP.

Both C3 WUE and C4 WUE were larger in the dry season than in the wet season for similar reasons as those explaining eWUE discussed above. The relative contributions to total GPP and T by the C3 and C4 components of the landscape resulted in much larger WUE for C4 grasses than Mulga trees, indicating the smaller stomatal conductance and larger photosynthetic rates of C4 grasses compared with C3 trees. In contrast, the difference in IWUE between wet and dry seasons was small (Fig. 7) because of the mediating effects of VPD. However, variations in IWUE can be overridden at annual timescales, which was found in the current study, through fluctuations in VPD and by compensation in stomatal conductance and GPP to changing conditions (Beer and others 2009). Such dependences of IWUE on environmental conditions indicate ecosystem physiology possesses an inherent ability to adaptively respond to environmental changes (Beer and others 2009).

In this semi-arid savanna woodland, simulated annual GPP followed a similar pattern to annual ET (Fig. 6), as a result of the intrinsic link between carbon and water fluxes via stomatal conductance

(Beer and others 2009; Leuning 1995; Niu and others 2008). This has also been observed in previous studies (Baldocchi 1994; Beer and others 2009). This linear coupling of GPP and ET resulted in relatively small variations in annual eWUE, ranging from between 0.80 and 1.46 g C m^{-2} (mm water)$^{-1}$ in 94% of simulated years, with an average of 1.17 g C m^{-2} (mm water)$^{-1}$ (Fig. 8). Although the SPA model has been validated for this site, there may still be many uncertainties in temporal interpolation of climate data and assumptions in wind speeds which may incur some errors on simulated GPP and ET, which therefore may introduce uncertainties into eWUE. However, the estimated annual mean average eWUE is comparable to those observed for other vegetation types. It was slightly larger than the global annual mean WUE for forests (0.95 g C m^{-2} (mm water)$^{-1}$), for grasslands (0.93 g C m^{-2} (mm water)$^{-1}$) and for deciduous broadleaf forests (0.87 g C m^{-2} (mm water)$^{-1}$), but is similar to evergreen conifer forests (1.15 g C m^{-2} (mm water)$^{-1}$) (Ponton and others 2006).

Over long-time scales (i.e. years to decades), the IWUE of mesic to wet ecosystems (500–3500 mm yr^{-1} precipitation) decreases with declining soil moisture, LAI and maximal leaf-level assimilation (Beer and others 2009). By contrast in the current study, four of the five wettest years were associated with minimal values in both forms eWUE and IWUE (Fig. 5 and Fig. 8) because ET responded more rapidly to increased precipitation than GPP, and consequently, the larger eWUE usually occurred in dry years. Similarly, Eamus and others (2013b) observed a seasonal increase of IWUE as soil moisture declined for this site Mulga woodland. Large inter-annual variations in precipitation and VPD may lead to large inter-annual variations in IWUE. Due to a larger mean VPD in a dry year than in a wet year, the eWUE in the dry year was increased more than in the wet year when it was normalized by VPD (calculation of IWUE). Consequently IWUE

showed larger year-to-year variations than eWUE.

Climate, GPP and ET

The climate in tropical Australia is characterized by strong coupling between precipitation and the Indian Ocean dipole (Saji and others 1999; Ihara and others 2008), which results in highly variable moisture availability (Van Etten 2009; Papalexiou and Koutsoyiannis 2013). Since the mid-1970s, the entire Indian Ocean has been warming, coinciding with a shift in climate regime over the Pacific Ocean (Ihara and others 2008). During the same period, average annual precipitation has increased and the occurrences of extreme precipitation events has increased, half of which occurred during the latter half of the period of this study (data not shown), which explained the increasing trend and larger variaility of simulated annual GPP and ET during this study period. With increasing amounts and variability of precipitation, carbon and water fluxes are expected to become larger in response to (1) a larger proportion of years that promote growth of C4 grasses; (2) carry-over of soil moisture storage for use by C3 trees during favorable conditions in dry years; and (3) higher IWUE at the seasonal time-scale and higher ecosystem WUE at the inter-annual timescale.

CONCLUSIONS

The modified SPA model successfully reproduced the seasonal evolution and inter-annual variability of measured gross primary productivity and evapotranspiration, by combining with the WAVES model through use of the LAI outputs of WAVES as inputs to SPA. Linking land surface exchange models with eco-physiological models is an effective way to explore ecosystem gas exchanges on decadal to century time-scales and has the potential to investigate possible impacts of future climate change on carbon and water fluxes of terrestiral ecosystems.

The strong seasonal and inter-annual variations in ecosystem carbon uptake and ET were driven by different climate factors. Maximal ecosystem carbon accumulation rates and ET occurred in the late wet season as a result of accumulation of sufficient soil moisture after intensive summer rainfall and the largest LAI. While the lowest GPP and ET occurred in the late dry season when water limitation was maximal and total LAI was minimal. As such we conclude that seasonality in meteorological variables of temperature, solar radiation, rainfall and vapour presser deficit cause seasonal responses in LAI and soil water, the latter of which drive seasonal patterns of GPP and ET. Simultaneously ecosystem water-use efficiency showed large seasonal variability as a result of the variations in these climate variables. Simulated annual GPP and ET varied substantially between years due to the effects of large inter-annual variability of precipitation and vapour presser deficit, ranging from 146.4 and 604.7 g C m^{-2} yr^{-1} for GPP and 110.2 to 625.8 mm yr^{-1} for ET. Average annual precipitation and occurrences of extreme precipitation events have increased during the latter half of the period of this study, which resulted in an increasing trend and larger variaility of annual GPP and ET during this period. Climate change, especially changes in annual precipitation and vapour pressure deficit, is likely to cause changes in annual budgets for carbon and water fluxes in this savanna ecosystem. The linear coupling of annual GPP to ET resulted in minimal year-to-year variation in ecosystem water-use efficiency.

ACKNOWLEDGEMENTS

This work was supported by grants from National Centre for Groundwater Research and Training (NCGRT) and the Australian Government's Terrestrial Ecosystems Research Network (TERN). This work was supported also by OzFlux and the Australian Supersite Network.

REFERENCES

590 Baldocchi DD. 1994. A comparative study of mass and energy exchange rates over a closed C3
591 (wheat) and an open C4 (corn) crop: II. CO_2 exchange and water use efficiency. Agric For
592 Meteorol 67(3): 291–321.
593 Baldocchi DD. 1997. Measuring and modelling carbon dioxide and water vapour exchange over a
594 temperate broad-leaved forest during the 1995 summer drought. Plant, Cell Environ 20: 1108.
595 Baldocchi DD. 2008. Breathing of the terrestrial biosphere: lessons learned from a global network
596 of carbon dioxide flux measurement systems. Aust J Bot 56: 1–26.
597 Baldocchi DD. Wilson KB. 2001. Modeling CO_2 and water vapuor exchange of a temperate
598 broadleaved forest across hourly to decadal time scales. Ecolo Model 142(1): 155–184.
599 Barton CVM, Duursma RA, Medlyn BE, Ellsworth DS, Eamus D, Tissue DT, Adams MA, Conroy
600 J, Crous KY, Liberloo M, Löw M, Linder S, McMurtrie RE. 2011. Effects of elevated
601 atmospheric [CO_2] on instantaneous transpiration efficiency at leaf and canopy scales in
602 Eucalyptus saligna. Global Change Biol 18: 585–595.
603 Beer C, Ciais P, Reichstein MD, Baldocchi D, Law BE, Papale D, Soussana JF, Ammann C,
604 Buchmann N, Frank D, Gianelle D, Janssens IA, Knohl A, Ko¨stner B, Moors E, Roupsard O,
605 Verbeeck H, Vesala T, Williams CA, Wohlfahrt G. 2009. Temporal and among-site variability of
606 inherent water use efficiency at the ecosystem level. Glob Biogeochem Cyc 23(2), GB2018,
607 doi:10.1029/2008GB003233.
608 Berry G, Reeder MJ, Jakob C. 2011. Physical mechanisms regulating summertime rainfall over
609 northwestern Australia. J Climate 24: 3705–3717.
610 Bowman D, Brown GK, Braby MF, Brown JR, Cook LG, Crisp MD, Ford F, Haberle S, Hughes J,
611 Isagi Y, Joseph L, McBride J, Nelson G, Ladiges PY. 2010. Biogeography of the Australian

monsoon tropics. J Biogeography 37: 201–216.

Chen C, Eamus D, Cleverly J, Boulain N, Cook P. 2014. Modelling vegetation water-use and groundwater recharge as affected by climate variability in an arid-zone Acacia savanna woodland. J Hydrology 519(2014): 1084–1096.

Chen XY, Bowler JM, Magee JW. 1991. Aeolian landscapes in central Australia: gypsiferous and quartz dune environments from Lake Amadeus. Sedimentology 38(3): 519–538.

Cleverly J. 2011. Alice Springs Mulga OzFlux site, OzFlux: Australian and New Zealand Flux Research and Monitoring Network, hdl: 102.100.100/8697.

Cleverly J, Boulain N, Villalobos-Vega R, Grant N, Faux R, Wood C, Cook PG, Yu Q, Leigh A, Eamus D. 2013. Dynamics of component carbon fluxes in a semi-arid Acacia woodland, central Australia. J Geophys Res-Biogeosciences 118(3): 1168–1185.

Collatz GJ, Ball JT, Grivet C, Berry JA. 1991. Physiological and environmental regulation of stomatal conductance, photosynthesis and transpiration: A model that includes a laminar boundary layer. Agric For Meteorol 54: 107–136.

Collatz GJ, Ribas-Carbo M, Berry JA. 1992. Coupled photosynthesis-stomatal conductance model for leaves of C_4 plants. Aus J Plant Physiol 19: 519–538.

Dawes W, Hatton TJ. 1993. Topog_IRM 1. Model description. CSIRO Division of Water Resources, Technical Memorandum 93: 33.

Dawes WR, Zhang L, Dyce P. 1998. WAVES V3.5 User Manual, CSIRO Land and Water, Canberra, ACT.

Eamus D. 2003. How does ecosystem water balance affect net primary productivity of woody ecosystems? Funct Plant Biol 30: 187–205.

634 Eamus D, Boulain N, Cleverly J, Breshears DD. 2013a. Global change-type drought-induced tree
635 mortality: vapuor pressure deficit is more important than temperature per se in causing decline in
636 tree health. Ecol Evol 3: 2711–2729.
637 Eamus D, Cleverly J, Boulain N, Grant N, Faux R, Villalobos-Vega R. 2013b. Carbon and water
638 fluxes in an arid-zone Acacia savanna woodland: An analyses of seasonal patterns and responses
639 to rainfall events. Agric For Meteorol 182–183: 225–238.
640 Eamus D, Cole S. 1997. Diurnal and seasonal comparsons of assimilation, phyllode conductance
641 and water potential of tree Acaia and one Eucalyptus species in the wet-dry tropics of Australia.
642 Aust J Bot 45: 275–290.
643 Eamus D, Prior L. 2001. Ecophysiology of trees of seasonally dry tropics: comparisons among
644 phenologies. Advan Ecol Res 32: 113–197.
645 Farquhar GD, von Caemmerer S, Berry JA. 1980. A biochemical model of photosynthetic CO_2
646 assimilation in leaves of C3 species. Planta 149: 78–90.
647 Fisher RA, Williams M, Lola da Costa A, Malhi Y, da Costa RF, Almeida S, Meir P (2007) The
648 response of an Eastern Amazonian rain forest to drought stress: results and modelling analyses
649 from a throughfall exclusion experiment. Glob Change Biol 13: 1–18.
650 Flanagan LB, Adkinson AC. 2011. Interacting controls on productivity in a northern Great Plains
651 grassland and implications for response to ENSO events. Glob Change Biol 17: 3293–3311.
652 Houghton JT, Meira Filho LG, Callander BA, Harris N, Kattenberg A, Maskell K. 1996. Climate
653 change 1995. The science of climate change. Cambridge University Press, Cambridge pp.572.
654 Ihara C, Kushnir Y, Cane MA. 2008. Warming trend of the Indian Ocean SST and Indian Ocean
655 dipole from 1880 to 2004. J Climate 21: 2035-2046.

IPCC. 2014. Working Group II contribution to the Fifth Assessment Report of the Intergovernmental Panel on Climate Change. Intergovernmental Panel on Climate Change, United Kingdom.

Jarvis PG, McNaughton KG. 1986. Stomatal control of transpiration: scaling up from leaf to region. Adv Ecol Res 15: 1–49.

Jeffrey SJ, Carter JO, Moodie KB, Beswick AR. 2001. Using spatial interpolation to construct a comprehensive archive of Australian climate data. Environ Model Software 16: 309–330.

Kong Q, Zhao S. 2010. Heavy rainfall caused by interactions between monsoon depression and middle-latitude systems in Australia: a case study. Meteor Atmos Phys 106: 205–226.

Landsberg JJ, Coops NC. 1999. Modeling forest productivity across large areas and long periods. Nat Res Model 12: 383–411.

Law BE, Falge E, Gu L, Baldocchi DD, Bakwin P, Berbigier P, Davis K, Dolman AJ, Falk M, Fuentes JD, Goldstein A, Granier A, Grelle A, Hollinger D, Janssens IA, Jarvis P, Jensen NO, Katul G, Mahli K, Matteucci G, Meyers T, Monson R, Munger W, Oechel W, Olson R, Pilegaard K, Paw UKT, Thorgeirsson H, Valentini R, Verma S, Vesala T, Wilson K, Wofsy S. 2002. Enviromental controls over carbon dioxide and water vapuor exchange of terrestrial vegetation. Agric For Meteorol 113: 97–120.

Leuning R. 1995. A critical appraisal of a combined stomatal-photosynthesis model for C3 plants. Plant Cell Environ 18(4): 339–355.

Linderson ML, Mikkelsen TN, Ibrom A, Lindroth A, Ro-Poulsen H, Pilegaard K. 2012. Up-scaling of water use efficiency from leaf to canopy as based on leafgas exchange relationships and the modelled in-canopy light distribution. Agric For Met 152: 201–211.

MacFarlane C, Hoffman M, Eamus D, Kerp N, Higginson S, McMurtrie R, Adams M. 2007. Estimation of leaf area index in eucalypt forest using digital photography. Agric For Meteorol 143: 176–188.

Migliavacca M, Meroni M, Manca G, Matteucci G, Montagnani L, Grassi G, Zenone T, Teobaldelli M, Goded I, Colombo R, Seufert G. 2009. Seasonal and interannual patterns of carbon and water fluxes of a poplar plantation under peculiar eco-climatic conditions. Agric For Meteorol 149(9): 1460–1476.

Monteith J, Unsworth M. 2008. Principles of Environmental Physics. Edward Arnold, London, UK pp250.

Morton SR, Stafford Smith DM, Dickman CR, Dunkerley DL, Friedel MH, McAllister RRJ, Reid JRW, Roshier DA, Smith MA, Walsh FJ, Wardle GM, Watson IW, Westoby M. 2011. A fresh framework for the ecology of arid Australia. J Arid Environ 75(4): 313–329.

Nemani RR, Keeling CD, Hashimoto H, Jolly WM, Piper SC, Tucker CJ, Myneni RB, Running SW. 2003. Climate-driven increases in global terrestrial net primary production from 1982 to 1999. Science 300(5625): 1560–1563.

Niu SL, Wu MY, Han Y, Xia JY, Li LH, Wan SQ. 2008. Water-mediatedresponses of ecosystem carbon fluxes to climatic change in a temperate steppe. New Phyt 177: 209–219.

Nix HA, Austin MP. 1973. Mulga: a bioclimatic analysis. Tropic Grassl 7: 9–20.

O'Grady AP, Cook PG, Eamus D, Duguid A, Wischusen JDH, Fass T, Worldege D. 2009. Convergence of tree water use within an arid-zone woodland. Oecologia 160: 643–655.

Papalexiou SM, Koutsoyiannis D. 2013. Battle of extreme value distributions: A global survey on extreme daily rainfall. Water Res Res 49: 10.

Perez-Ruiz ER, Garatuza-Payan J, Watts CJ, Rodriguez JC, Yepez EA, Scott RL. 2010. Carbon dioxide and water vapour exchange in a tropical dry forestinfluenced by the North American Monsoon System (NAMS). J Arid Environ 74: 556–563.

Ponce-Campos GE, Moran MS, Huete A, Zhang Y, Bresloff C, Huxman TE, Eamus D, Bosch DD, Buda AR, Gunter SA, Scalley TH, Kitchen SG, McClaran MP, McNab WH, Montoya DS, Morgan JA, Peters DPC, Sadler JE, Seyfried MS, Starks PJ. 2013. Ecosystem resilience despite large-scale altered hydroclimatic conditions. Nature 494: 349–352.

Ponton S, Flanagan LB, Alstad KP, Johnson BG, Morgenstern K, Kljun N, Black TA, Barr AG. 2006. Comparison of ecosystem water-use efficiency among Douglas-fir forest, aspen forest and grassland using eddy covariance and carbon isotope techniques. Global Change Biol 12: 294–310.

Raz-Yaseef N, Yakir D, Schiller G, Cohen S. 2012. Dynamics of evapotranspiration partitioning in a semi-arid forest as affected by temporal rainfall patterns. Agric For Meteorol 157: 77–85.

Running SW, Coughlan JC. 1988. A general model of forest ecosystem processes for regional applications. 1. Hydrological balance, canopy gas exchange and primary production processes. Ecolo Model 42: 125-154.

Saji NH, Goswami BN, Vinayachandran PN, Yamagata T. 1999. A dipole mode in the tropical Indian Ocean. Nature 401: 360–363.

Salinger MJ. 2005. Climate variability and change: past, present and future-an overview. Climatic Change 70(1-2): 9–29.

Schwarz PA, Law BE, Williams M, Irvine J, Kurpius M, Moore D. 2004. Climatic versus biotic constraints on carbon and water fluxes in seasonally drought-affected ponderosa pine ecosystems.

722 Global Biogeochem Cyc 18: 1–17.

723 Shao MA, Huang M, Zhang L, Li YS. 2002. Simulation of field-scale water balance on the Loess
724 Plateau using the WAVES model. ACIAR Mono Ser 84: 48–56.

725 Tian H, Melillo JM, Kicklighter DW, McGuire AD, Helfrich Iii J, Moore Iii B, Vörösmarty CJ.
726 2000. Climatic and biotic controls on annual carbon storage in Amazonian ecosystems. Global
727 Ecol Biogeogr 9(4): 315-335.

728 Twine TE, Kustas WP, Norman JM, Cook DR, Houser PR, Meyers TP, Prueger JH, Starks PJ,
729 Wesley ML. 2000. Correcting eddy-covariance flux underestimates over a grassland. Agric For
730 Meteorol 103: 279–300.

731 Van Etten EJB. 2009. Inter-annual rainfall variability of arid Australia: Greater than elsewhere?
732 Aust Geogr 40: 109–120.

733 Wang H, Zhang L, Dawes WR, Liu C. 2001. Improving water use efficiency of irrigated crops in
734 the North China Plain—measurements and modelling. Agric Water Manage 48(2): 151–167.

735 Wang X, Wang C, Yu G. 2008. Spatio-temporal patterns of forest carbon dioxide exchange based
736 on global eddy covariance measurements. Sci China Ser D: Earth Sci 51: 1129–1143.

737 Weiss M, Baret F, Smith GJ, Jonckheere I, Coppin P. 2004. Reviewof methods for in situ leaf area
738 index (LAI) determination Part II, Estimation of LAI, errors and sampling. Agric For Meteorol
739 121: 37–53.

740 Whitley RJ, Macinnis-Ng CM, Hutley LB, Beringer J, Zeppel M, Williams M, Taylor D, Eamus, D.
741 2011. Is productivity of mesic savannas light limited or water limited? Results of a simulation
742 study. Glob Change Biol 17(10): 3130–3149.

743 Williams M, Eugster W, Rastetter EB, Mcfadden JP, Chapin Iii FS. 2000. The controls on net

ecosystem productivity along an Arctic transect: a model comparison with flux measurements. Glob Change Biol 6(S1): 116–126.

Williams M, Law BE, Anthoni PM, Unsworth MH. 2001a. Use of a simulation model and ecosystem flux data to examine carbon-water interactions in Ponderosa pine. Tree Phys 21: 287–298.

Williams M, Rastetter EB, Shaver GR, Hobbie JE, Carpino E, Kwiatkowski B. 2001b. Primary production of an Arctic watershed: an uncertainty analysis. Ecol Appl 11 (6): 1800–1816.

Williams M, Malhi Y, Nobre AD, Rastetter EB, Grace J, Pereira MGP. 1998. Seasonal variation in net carbon exchange and evapotranspiration in a Brazilian rain forest: a modelling analysis. Plant Cell Environ 21(10): 953–968.

Williams M, Rastetter EB, Fernandes DN, Goulden ML, Wofsy SC, Shaver GR, Melillo JM, Munger JW, Fan SM, Nadelhoffer KJ. 1996. Modelling the soil-plant-atmosphere continuum in a Quercus-Acer stand at Harvard Forest: the regulation of stomatal conductance by light, nitrogen and soil/plant hydraulic properties. Plant Cell Environ 19(8): 911–927.

Wilson K, Goldstein A, Falge E, Aubinet M, Baldocchi D, Berbigier P, Bernhofer C, Ceulemans R, Dolman H, Field C, Grelle A, Ibrom A, Law BE, Kowalski A, Meyers T, Moncrieff J, Monson R, Oechel W, Tenhunen J, Verma S, Valentini R. 2002. Energy balance closure at FLUXNET sites. Agric For Meteorol 113: 223–243.

Winkworth RE. 1973. Eco-physiology of Mulga (Acacia aneura). Tropic Grassl 7(1): 43–48.

Wohlfahrt G, Fenstermaker LF, Arnone JA. 2008. Large annual net ecosystem CO_2 uptake of a Mojave Desert ecosystem. Glob Change Biol 14: 1475–1487.

Wu H, Rykiel Jr EJ, Hatton T, Walker J. 1994. An integrated rate methodology (IRM) for

multi-factor growth rate modelling. Ecol Model 73: 97–116.

Yan LM, Chen SP, Huang JH, Lin GH. 2011. Water regulated effects of photosynthetic substrate supply on soil respiration in a semiarid steppe. Glob Change Biol 17: 1990–2001.

Zeppel M, Macinnis-Ng C, Palmer A, Taylor D, Whitley R, Fuentes S, Yunusa I, Williams M, Eamus D. 2008. An analysis of the sensitivity of sap flux to soil and plant variables assessed for an Australian woodland using a soil–plant–atmosphere model. Funct Plant Biol 35 (6): 509–520.

Zhang L, Dawes WR (Eds). 1998. WAVES-An Integrated Energy and Water Balance Model. Technical Report No. 31/98, CSIRO Land and Water, Canberra, Australia.

Zhang L, Dawes WR, Hatton TJ. 1996. Modelling hydrologic processes using a biophysically based model application of WAVES to FIFE and HAPEX-MOBILHY. J Hydrology 185: 147–169.

Zhang L, Dawes WR, Slavich PG, Meyer WS, Thorburn PJ, Smith DJ, Walker GR. 1999. Growth and ground water uptake responses of lucerne to changes in groundwater levels and salinity: lysimeter, isotope and modelling studies. Agric Water Manage 39(2): 265–282.

781 **Figure Legends**

782 Figure 1. Comparison of total leaf area index (LAI) from field measurements, MODIS and
783 simulations (a). Comparison of measured and simulated break down of canopy (b) and understory
784 (c) LAI.

785 Figure 2. Comparison of measured and simulated daily ET (a) and GPP (b) at Alice Spring flux
786 station from 3 Sep 2010 to 30 Jun 2013.

787 Figure 3. Monthly mean air temperature (a), monthly mean solar radiation (b), monthly
788 precipitation (c) and monthly mean vapour pressure deficit (VPD) (d) during 1981−2012 at
789 Territory Grape Farm Station obtained from SILO (Jeffrey and others 2001). The error bar
790 indicates the ranges of monthly mean air temperature, mean solar radiation, monthly precipitation
791 or monthly mean VPD during 1981−2012 for each month.

792 Figure 4. (a) Simulated seasonal dynamics of gross primary productivity (GPP) and (c) the
793 corresponding contributions of tree (C3) and understory (C4); (b) Simulated seasonal dynamics
794 of ecosystem evapotranspiration (ET) and (d) transpiration (T) of C3 and C4 during 1981–2012.
795 The dotted–solid lines represent the mean monthly values averaged over the period 1981-2012.
796 The error bars indicate the range of monthly GPP and ET for each month during 1981−2012.

797 Figure 5. Mean annual temperature (a), mean annual solar radiation (b), annual precipitation (c)
798 and mean annual vapour pressure deficit (VPD; d) during 1981–2012.

799 Figure 6. (a) Simulated total annual GPP and the corresponding contributions of C3 and C4; (b)
800 Simulated total annual ET and transpiration (T) of C3 and C4 during 1981–2012.

801 Figure 7. Simulated mean seasonal variations of ecosystem water-use-efficiency (eWUE), inherent
802 water-use-efficiency (IWUE), WUE for C3 trees (C3 WUE) and WUE for C4 grasses (C4 WUE)
803 during 1981–2012.

Figure 8. Simulated annual mean water-use-efficiency (eWUE), annual mean inherent water-use-efficiency (IWUE), eWUE for C3 trees (C3 WUE) and eWUE for C4 grasses (C4 WUE) during 1981–2012.

Figure 9. The Average monthly (Jan-Dec) GPP (a, c) and ET (b, d) as a function of average monthly (Jan-Dec) total LAI (upper panel) and soil moisture content (lower panel) during 1981–2012. ** indicates $p < 0.01$.

Figure 10. Simulated monthly mean LAI of the canopy (C3), understory (C4) and their total during 1981−2012, obtained from Chen *et al.* (2014).

Figure 11. The linear/curvilinear relationship between annual total GPP (solid line) and ET (dashed line) and precipitation (a), vapour presser deficit (VPD; b) and temperature (c). **indicates $p < 0.01$; *indicates $p < 0.05$.

Figure 12. Simulated seasonal dynamics of gross primary productivity (GPP; a) and ecosystem evapotranspiration (ET; b) in dry (less than 25% of the precipitation percentiles) and wet (higher than 75% of the precipitation percentiles) years during 1981–2012.

Figure 13. The difference between simulated annual ET and precipitation as a function of annual precipitation during 1981–2012 (a). The difference between simulated annual ET and precipitation as a function of the previous year's precipitation during 1981–2011 (b). A positive difference (ET exceeded rainfall) means there was carry-over of water in a given year and this effect was largest when dry years followed wet years. ** indicates $p < 0.01$.

Table Legends

Table 1: Parameter/variable values used in soil-plant atmosphere (SPA) for this study.

Table 2: The coefficient of determination (r^2), root mean square error (RMSE) and model efficiency (ME) of simulated ET and GPP.

Table 3: The linear relationship between average monthly gross primary productivity (GPP), evapotranspiration (ET) and temperature (T), precipitation (P), solar radiation (SR), vapour presser deficit (VPD) and the linear relationship between ecosystem water-use efficiency (eWUE) and T, P, SR, VPD and average total LAI (LAI) and soil water content (SW) during 1981–2012. ** indicates $p < 0.01$.

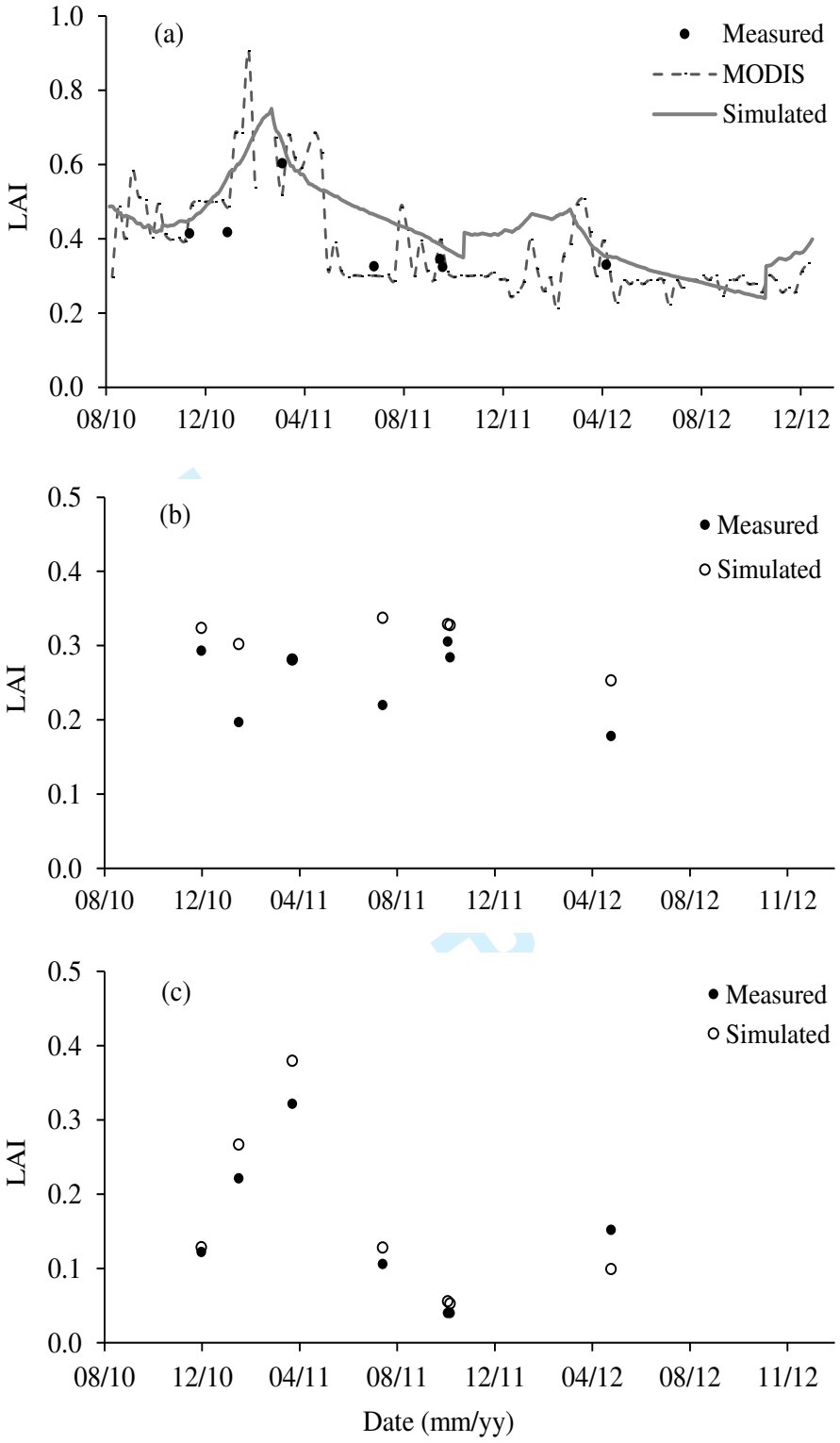
(a)
Measured
MODIS
Simulated
LAI
1.0
0.8
0.6
0.4
0.2
0.0
08/10
12/10
04/11
08/11
12/11
04/12
08/12
12/12
(b)
Measured
Simulated
LAI
0.5
0.4
0.3
0.2
0.1
0.0
08/10
12/10
04/11
08/11
12/11
04/12
08/12
11/12
(c)
Measured
Simulated
LAI
0.5
0.4
0.3
0.2
0.1
0.0
08/10
12/10
04/11
08/11
12/11
04/12
08/12
11/12
Date (mm/yy)

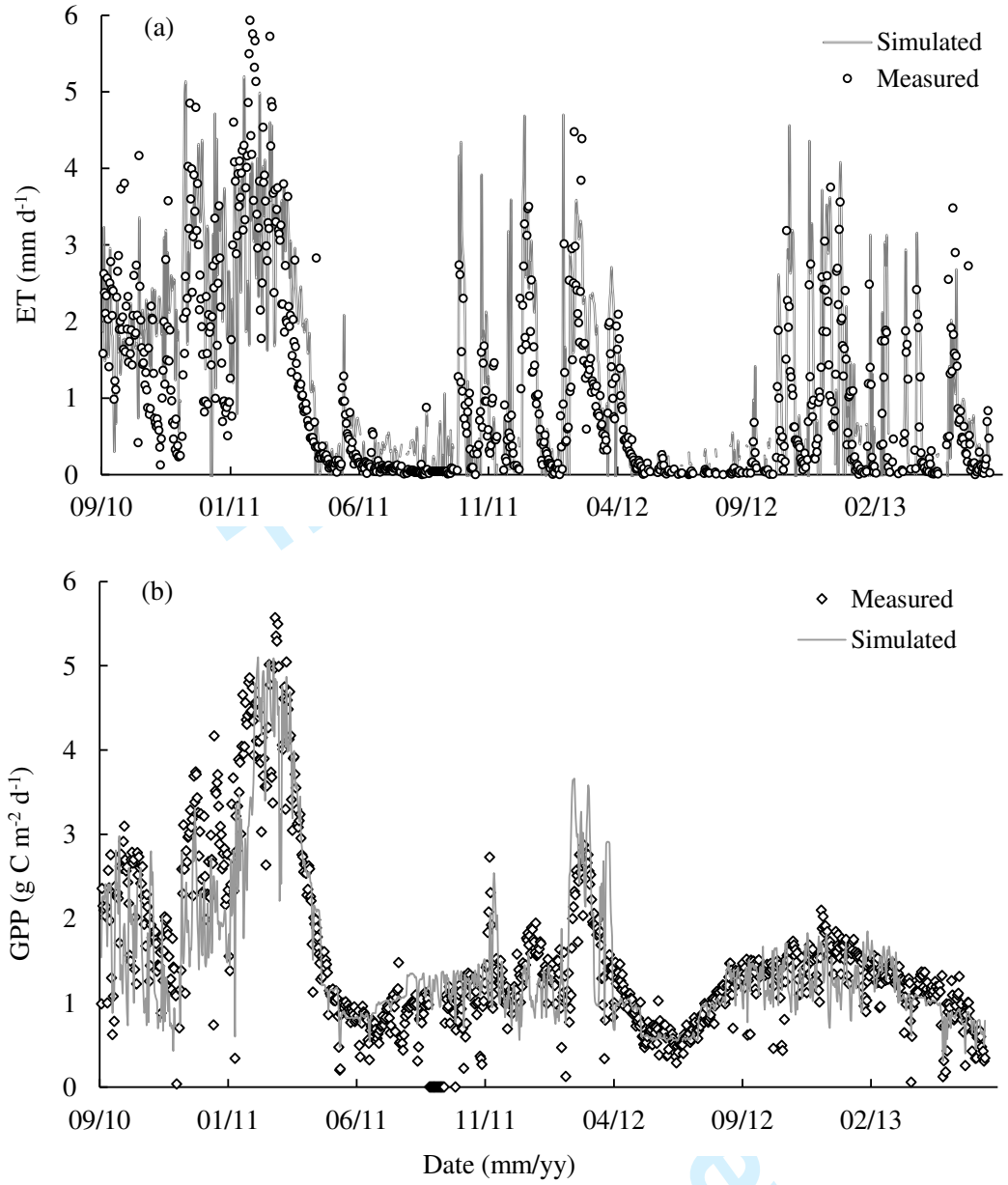
(a)
Simulated
Measured
ET (mm d-1)
0
1
2
3
4
5
6
09/10
01/11
06/11
11/11
04/12
09/12
02/13
(b)
Measured
Simulated
GPP (g C m-2 d-1)
0
1
2
3
4
5
6
09/10
01/11
06/11
11/11
04/12
09/12
02/13
Date (mm/yy)

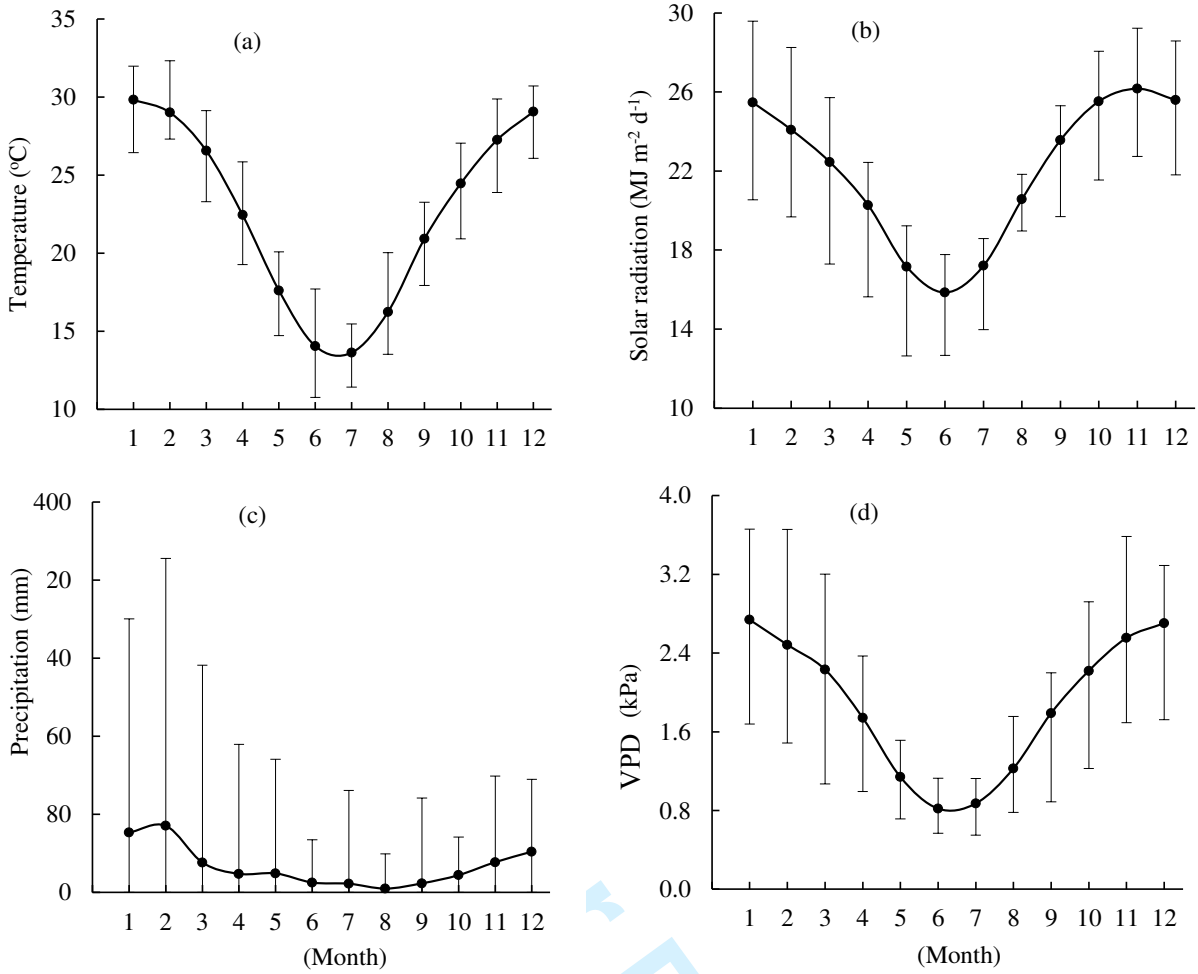
(a)
Temperature (°C)
35
30
25
20
15
10
1 2 3 4 5 6 7 8 9 10 11 12
(b)
Solar radiation (MJ m-2 d-1)
30
26
22
18
14
10
1 2 3 4 5 6 7 8 9 10 11 12
(c)
Precipitation (mm)
400
20
40
60
80
0
1 2 3 4 5 6 7 8 9 10 11 12
(Month)
(d)
VPD (kPa)
4.0
3.2
2.4
1.6
0.8
0.0
1 2 3 4 5 6 7 8 9 10 11 12
(Month)

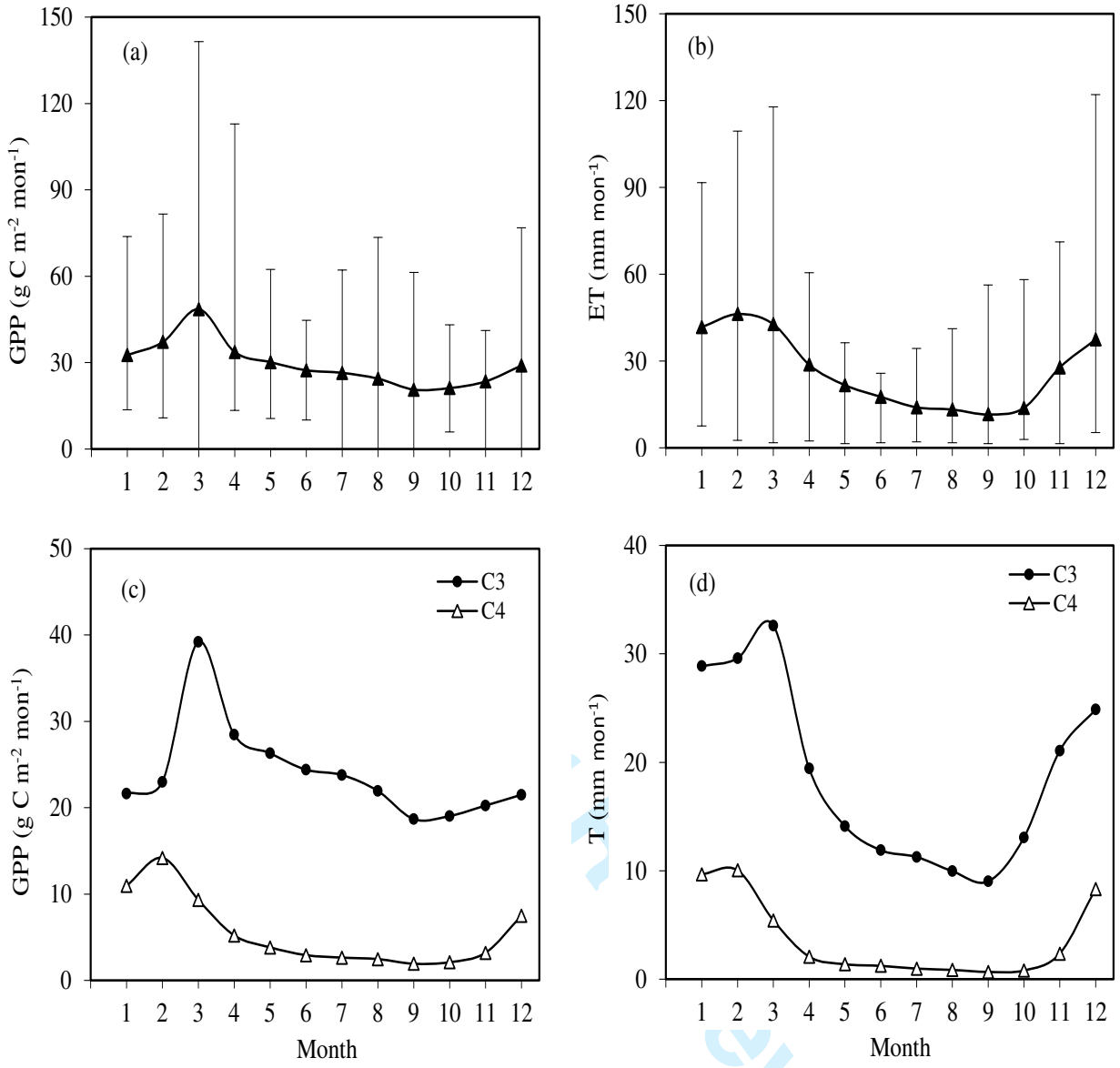
(a)
GPP (g C m-2 mon-1)
(b)
ET (mm mon-1)
(c)
GPP (g C m-2 mon-1)
C3
C4
Month
(d)
T (mm mon-1)
C3
C4
Month

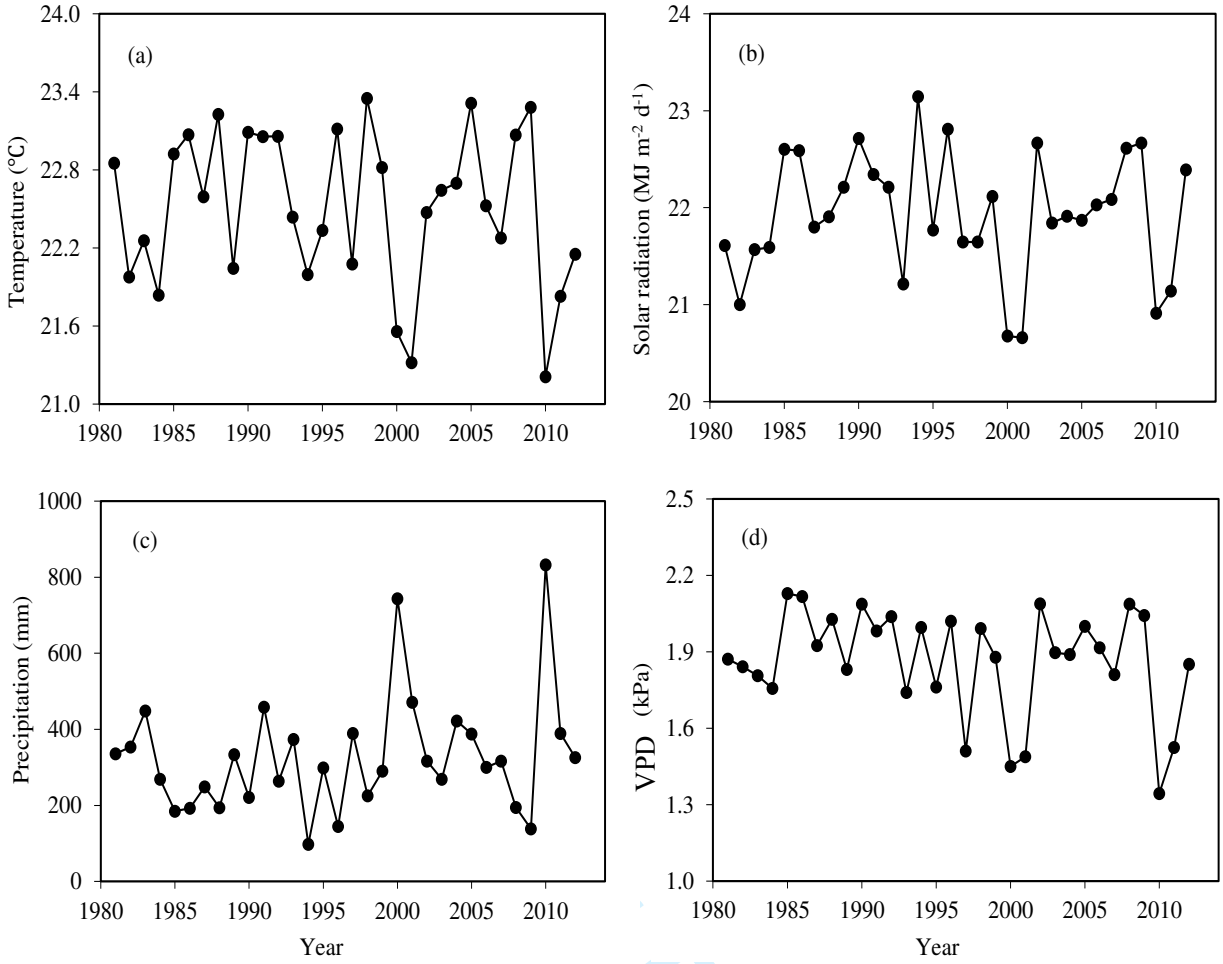
(a)
Temperature (°C)
24.0
23.4
22.8
22.2
21.6
21.0
(b)
Solar radiation (MJ m-2 d-1)
24
23
22
21
20
(c)
Precipitation (mm)
1000
800
600
400
200
0
(d)
VPD (kPa)
2.5
2.2
1.9
1.6
1.3
1.0
1980 1985 1990 1995 2000 2005 2010
Year

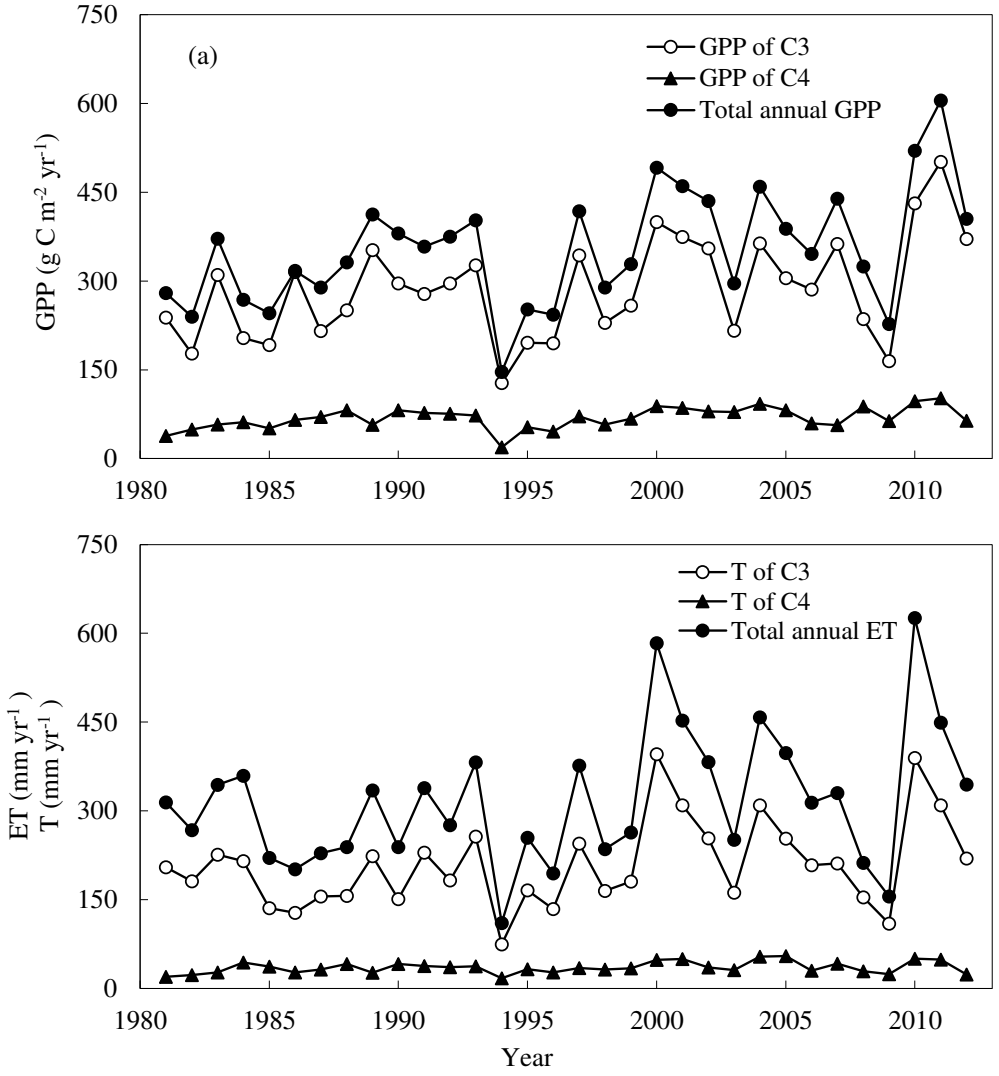
(a)
GPP of C3
GPP of C4
Total annual GPP
GPP (g C m-2 yr-1)
750
600
450
300
150
0
1980
1985
1990
1995
2000
2005
2010
T of C3
T of C4
Total annual ET
ET (mm yr-1)
T (mm yr-1)
Year

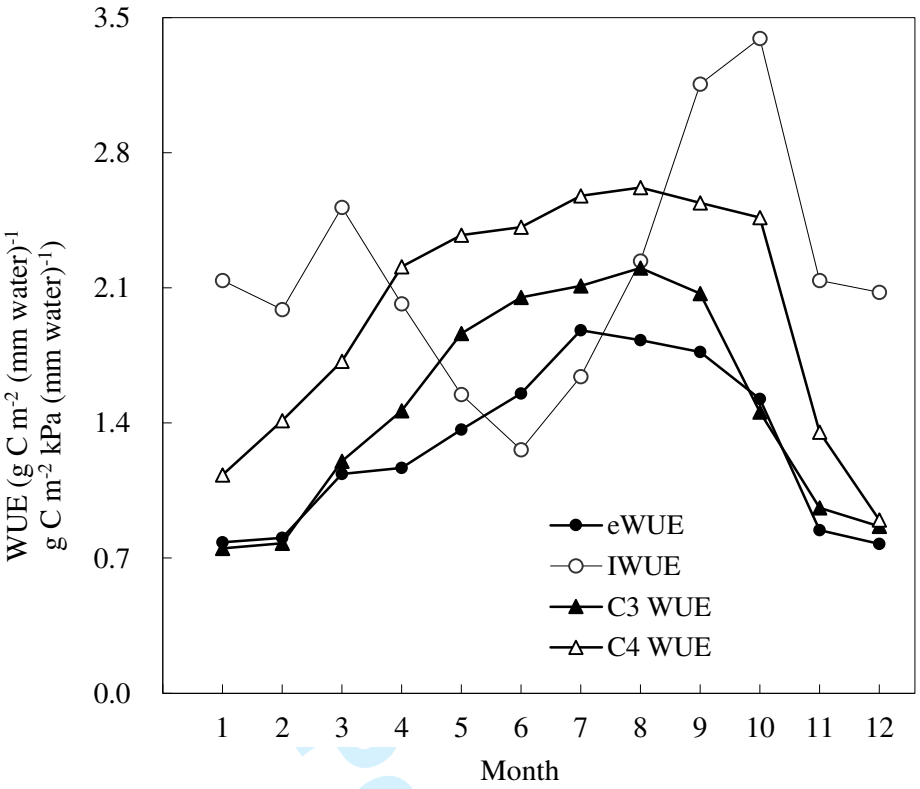

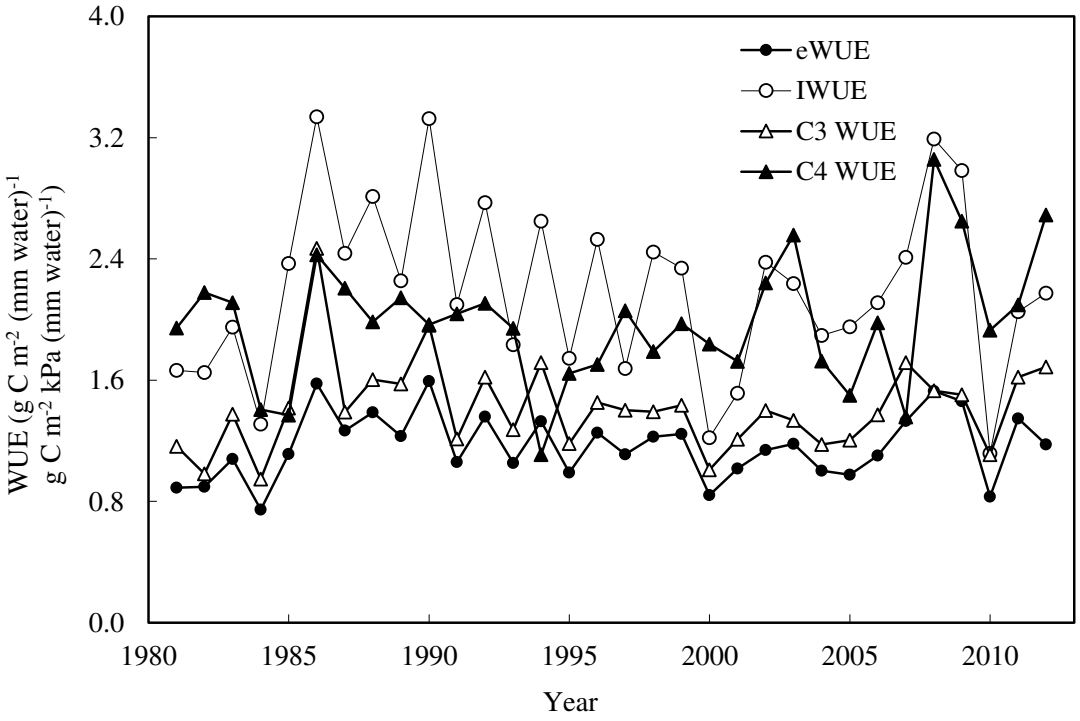

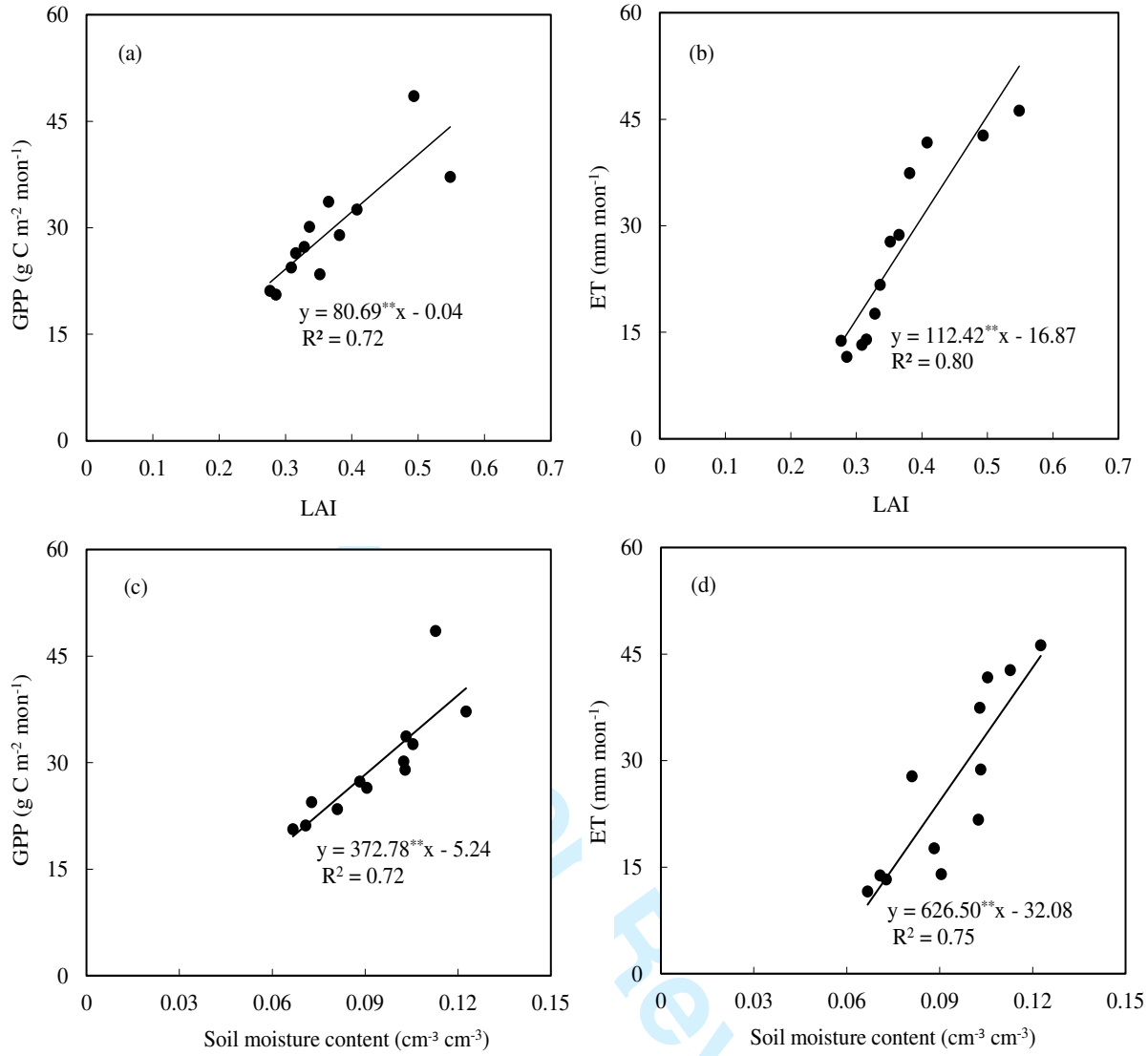
(a)
GPP (g C m-2 mon-1)
y = 80.69**x - 0.04
R² = 0.72
LAI
(b)
ET (mm mon-1)
y = 112.42**x - 16.87
R² = 0.80
LAI
(c)
GPP (g C m-2 mon-1)
y = 372.78**x - 5.24
R² = 0.72
Soil moisture content (cm-3 cm-3)
(d)
ET (mm mon-1)
y = 626.50**x - 32.08
R² = 0.75
Soil moisture content (cm-3 cm-3)

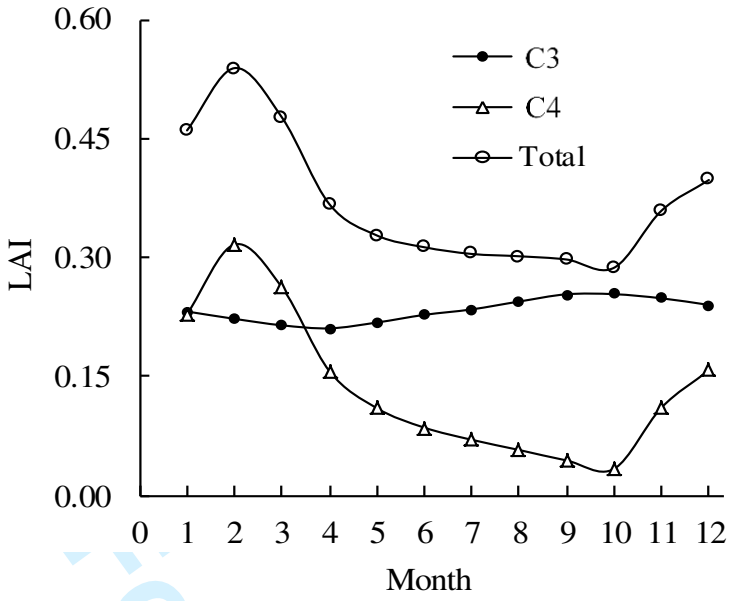

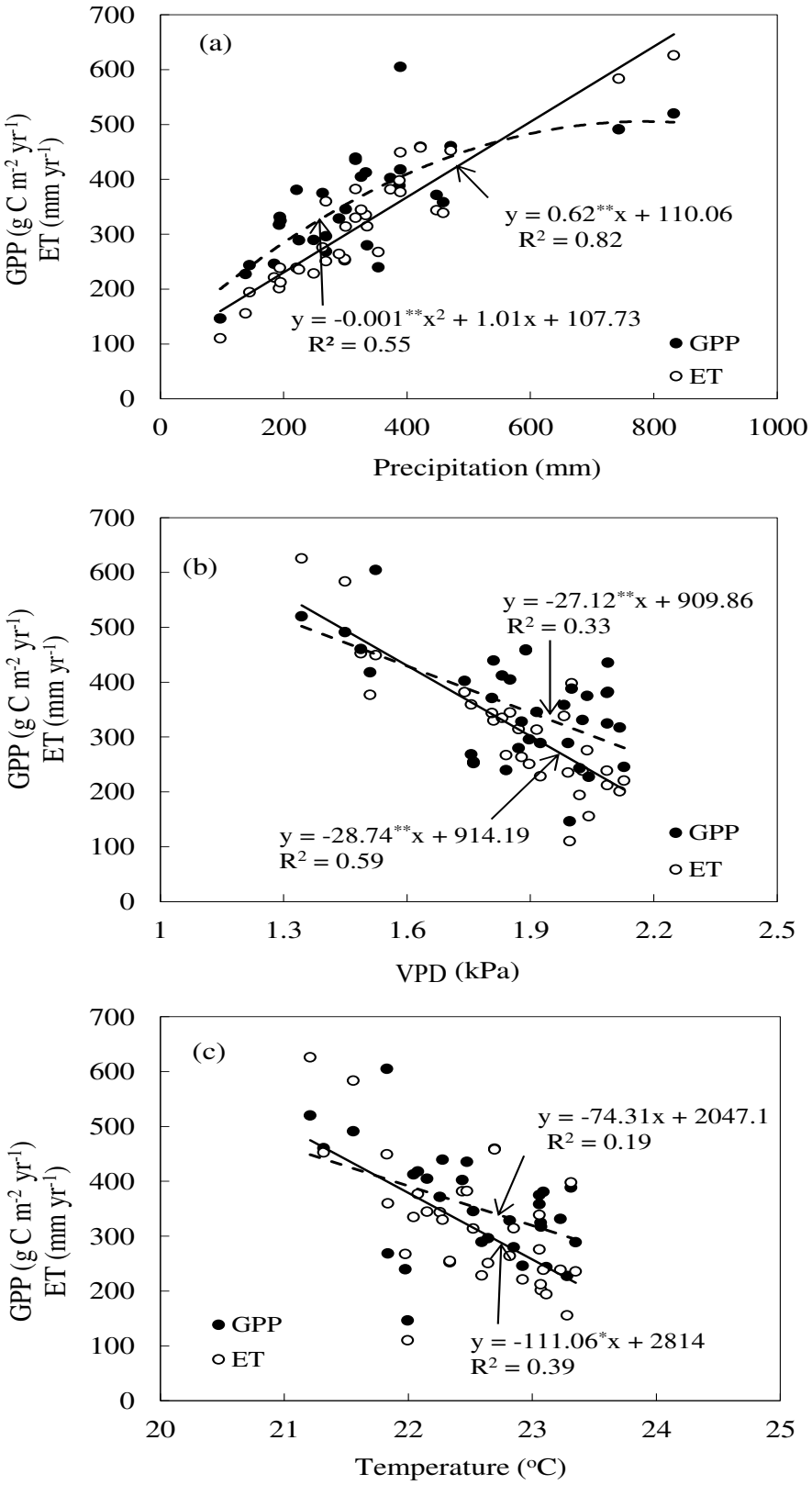
(a)
GPP (g C m-2 yr-1)
ET (mm yr-1)
y = 0.62**x + 110.06
R² = 0.82
y = -0.001**x² + 1.01x + 107.73
R² = 0.55
GPP
ET
Precipitation (mm)
(b)
y = -27.12**x + 909.86
R² = 0.33
y = -28.74**x + 914.19
R² = 0.59
VPD (kPa)
(c)
y = -74.31x + 2047.1
R² = 0.19
y = -111.06*x + 2814
R² = 0.39
Temperature (°C)

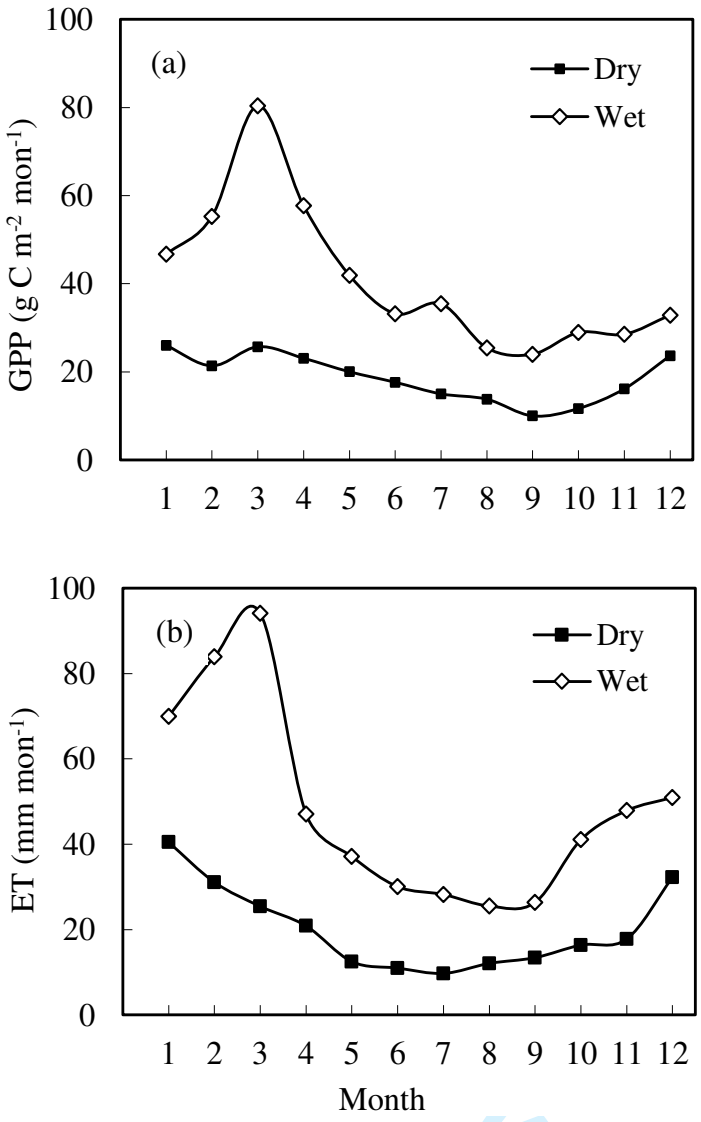
(a)
Dry
Wet
GPP (g C m-2 mon-1)
100
80
60
40
20
0
1 2 3 4 5 6 7 8 9 10 11 12
(b)
Dry
Wet
ET (mm mon-1)
100
80
60
40
20
0
1 2 3 4 5 6 7 8 9 10 11 12
Month

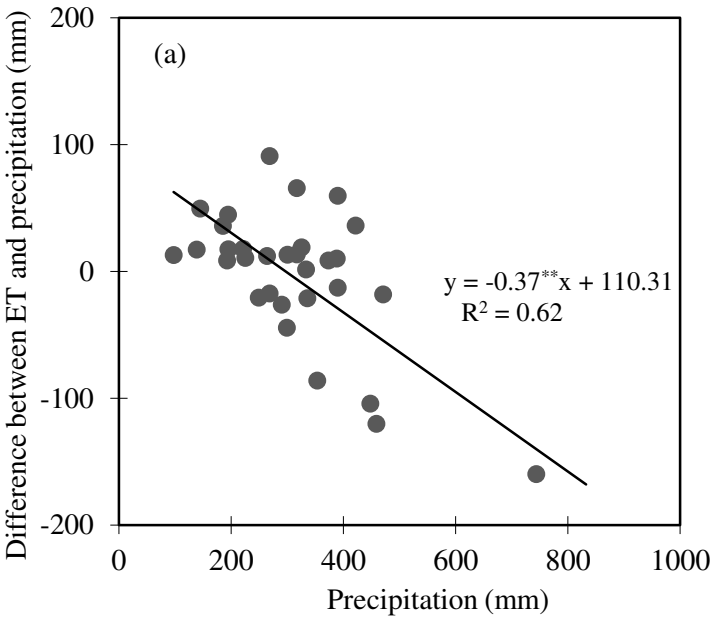
(a)
Difference between ET and precipitation (mm)
200
100
0
-100
-200
0
200
400
600
800
1000
Precipitation (mm)
y = -0.37**x + 110.31
R2 = 0.62

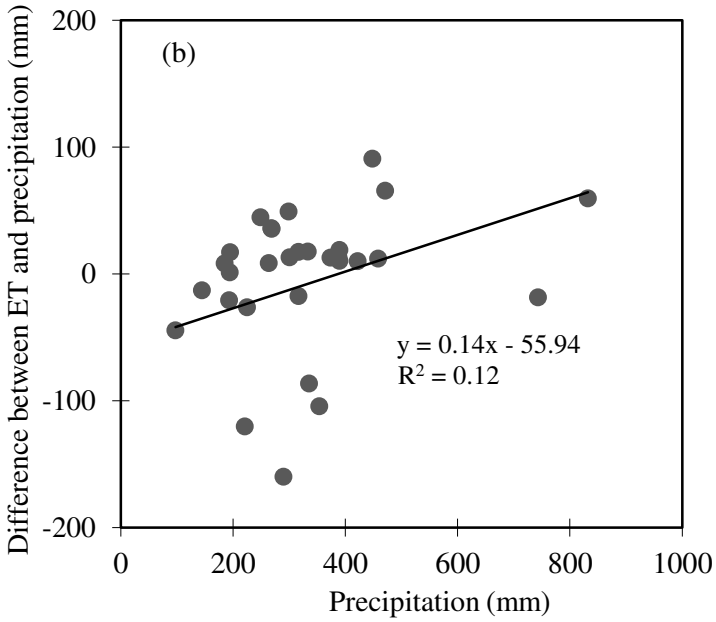
(b)
Difference between ET and precipitation (mm)
200
100
0
-100
-200
0
200
400
600
800
1000
Precipitation (mm)
y = 0.14x - 55.94
R2 = 0.12

Table 1: Parameter/variable values used in SPA

Parameter/variable	Symbol	Units	Value	Source
Meteorology				
Air temperature	T_a	°C	Variable	Extracted from SILO (Jeffrey *et al.*, 2001) and measured
Precipitation	P	mm		
Solar radiation	S	W m^{-2}		
Vapour presser deficit	VPD	hPa		
Photosynthetically active radiation	PAR		Variable	Calculated based on solar radiation
Wind speed	W	m/s	Variable	Measured and estimated
Soil				
Layer height of soil	HS	m	0.1–1.0m, then 1.1-4 m	Site estimated
% soil clay content in top 10 cm		%	15	Measured
% soil sand content in top 10 cm		%	74	Measured
Organic matter content in top 10 cm		%	20	Measured
Soil water potential	Ψ_s	MPa	-3	Predawn leaf water potential
Initial soil water content		cm^{-3} cm^{-3}	Variable	Measured
Root biomass		g	1500	Pressland (1975)
Rooting depth		m	4	Hill and Hill (2003), Anderson *et al.* (2008) and Barron *et al.* (2012)
Biophysics				
Canopy layer capacitance	C_n	mmol $layer^{-1}$ MPa^{-1}	5000	Williams *et al.* (1996)
Canopy hydraulic conductivity	G_{plant}	mmol m^{-1} s^{-1} MP^{-1}	3.5	Zeppel *et al.* (2008)
Leaf area index	LAI	m^{-2} m^{-2}	0.13–0.97	Simulated by WAVES and measured
Dimension of leaves		m^2	0.08	Prior *et al.* (1997)
Minimum sustainable leaf water potential	Ψ_{lmin}	MPa	-20	Measured

Continued: Table 1: Parameter/variable values used in SPA

Areal concentration of leaf N	N	g m^{-2}	2.9	Evans *et al.* (2000)
Proportion of total canopy N in top layer	N_{top}		0.1	Site estimated
Leaf temperature	T_i	°C	Variable	Extracted from SILO (Jeffrey *et al.*, 2001) and measured
C3 RuBP carboxylation capacity	C3, V_{cmax}	µmol m^{-2} s^{-1}	30.4	Adjusted based on the value in Whitely *et al.* (2011)
C3 maximum electron transport rate	C3, J_{max}	µmol m^{-2} s^{-1}	50.1	
C4 RuBP carboxylation capacity	C4, V_{cmax}	µmol m^{-2} s^{-1}	26.3	
$\delta A/\delta g_s$ threshold for stomatal opening	ι	%	1.0007	Williams *et al.* (1996)
Root resistivity		MPa s g mol^{-1}	100	Whitely *et al.* (2011)
Fine root radius	r_r	m	0.0001	Measured

Table 2: The r^2, RMSE and ME of simulated ET and GPP.

Item	Observed range (mean)	Simulated range (mean)	r^2	RMSE	ME
ET (mm d^{-1})	0.0−5.93 (1.15)	0.0−5.31 (1.29)	0.71	0.86	0.90
GPP (g C m^{-2} d^{-1})	0−5.57 (1.52)	0.09−5.43 (1.49)	0.80	0.45	0.79

Table 3: Relationship between GPP, ET, WUE and climate factors, LAI and SW

Factors	r^2	Factors	r^2
GPP-T	0.13	eWUE-T	0.90**
GPP-P	0.23	eWUE-P	0.51**
GPP-SR	0.001	eWUE-SR	0.94**
GPP-D	0.06	eWUE-D	0.96**
ET-T	0.59**	eWUE-LAI	0.14
ET-P	0.70**	eWUE-SW	0.03
ET-SR	0.18		
ET-D	0.42**		